Molecular Therapy
Original Article

Polymer-Mediated Inhibition of Pro-invasive Nucleic Acid DAMPs and Microvesicles Limits Pancreatic Cancer Metastasis

Ibtehaj Naqvi,[1,2,3,8] Ruwan Gunaratne,[1,2,3,8] Jessica E. McDade,[3] Angelo Moreno,[3] Rachel E. Rempel,[3] Douglas C. Rouse,[4] Silvia Gabriela Herrera,[5] David S. Pisetsky,[6] Jaewoo Lee,[3] Rebekah R. White,[3,7] and Bruce A. Sullenger[1,3]

[1]Department of Pharmacology and Cancer Biology, Duke University, Durham, NC 27710, USA; [2]Medical Scientist Training Program, Duke University, Durham, NC 27710, USA; [3]Department of Surgery, Duke University, Durham, NC 27710, USA; [4]Division of Laboratory Animal Resources, Duke University, Durham, NC 27710, USA; [5]Department of Pharmacology, University of North Carolina, Chapel Hill, NC 27514, USA; [6]Department of Medicine, Duke University, Durham, NC 27710, USA; [7]Department of Surgery, University of California San Diego, La Jolla, CA 92093, USA

Nucleic acid binding polymers (NABPs) have been extensively used as vehicles for DNA and RNA delivery. More recently, we discovered that a subset of these NABPs can also serve as anti-inflammatory agents by capturing pro-inflammatory extracellular nucleic acids and associated protein complexes that promote activation of toll-like receptors (TLRs) in diseases such as lupus erythematosus. Nucleic-acid-mediated TLR signaling also facilitates tumor progression and metastasis in several cancers, including pancreatic cancer (PC). In addition, extracellular DNA and RNA circulate on or within lipid microvesicles, such as microparticles or exosomes, which also promote metastasis by inducing pro-tumorigenic signaling in cancer cells and pre-conditioning secondary sites for metastatic establishment. Here, we explore the use of an NABP, the 3rd generation polyamidoamine dendrimer (PAMAM-G3), as an anti-metastatic agent. We show that PAMAM-G3 not only inhibits nucleic-acid-mediated activation of TLRs and invasion of PC tumor cells *in vitro*, but can also directly bind extracellular microvesicles to neutralize their pro-invasive effects as well. Moreover, we demonstrate that PAMAM-G3 dramatically reduces liver metastases in a syngeneic murine model of PC. Our findings identify a promising therapeutic application of NABPs for combating metastatic disease in PC and potentially other malignancies.

INTRODUCTION

Nucleic acid binding polymers (NABPs) have been widely utilized as vehicles for DNA and RNA delivery.[1] Recently, our laboratory discovered that a subset of such polymers can also serve as anti-inflammatory agents that capture pro-inflammatory extracellular nucleic acids and neutralize their activation of the nucleic-acid-sensing toll-like family of receptors (TLRs).[2] Although TLRs evolved to provide innate immunity against infection by recognizing pathogen associated molecular patterns (PAMPs), they can also be activated by endogenous damage associated molecular patterns (DAMPs), such as nucleic acids and nucleic-acid-protein complexes released by dead and dying cells.[3,4] Excessive activation of TLRs contributes to disease progression in several autoimmune or inflammatory disorders.[4] We previously demonstrated that certain NABPs, such as the 3rd generation polyamidoamine dendrimer (PAMAM-G3), can bind pro-inflammatory extracellular nucleic acids and nucleic-acid-protein complexes and prevent subsequent TLR activation[2] and improve outcomes in animal models of lupus, acute liver failure, and influenza infection[2,5] without evidence of systemic toxicity.

An additional pathological role for inappropriate TLR activation in tumor progression and metastasis has now been established. For example, TLR signaling in lung cancer leads to increased angiogenesis and tumor cell invasion.[6] TLR agonists also promote increased tumor invasion *in vitro* in breast cancer and metastasis *in vivo* in pancreatic and colorectal cancer.[7–9] Moreover, circulating levels of innate TLR agonists, including cell-free nucleic acids and associated complexes, are elevated in a multitude of cancers and can further increase following chemotherapy, radiation, and surgery.[9–12] These endogenous factors can circulate alone or on/within lipid microvesicles, such as microparticles or exosomes, to induce pro-tumorigenic signaling in cancer cells and the tumor microenvironment and precondition secondary sites for metastatic establishment.[6–8,13–17]

Recent work has highlighted specific contributions of TLR activation mediated by circulating nucleic acid DAMPs to disease progression in pancreatic cancer (PC),[7,13,15] which has the worst prognosis of all major cancers due in part to its aggressive, metastatic nature.[18,19] Surgical resection is the only potentially curative treatment option.

Received 30 August 2017; accepted 18 February 2018;
https://doi.org/10.1016/j.ymthe.2018.02.018.

[8]These authors contributed equally to this work.

Correspondence: Rebekah R. White, Department of Surgery, Duke University, Durham, NC 27710, USA.
E-mail: rewhite@ucsd.edu
Correspondence: Bruce A. Sullenger, Department of Surgery, Duke University, MSRB II Room 1079, 106 Research Drive, Durham, NC 27710, USA.
E-mail: bruce.sullenger@duke.edu

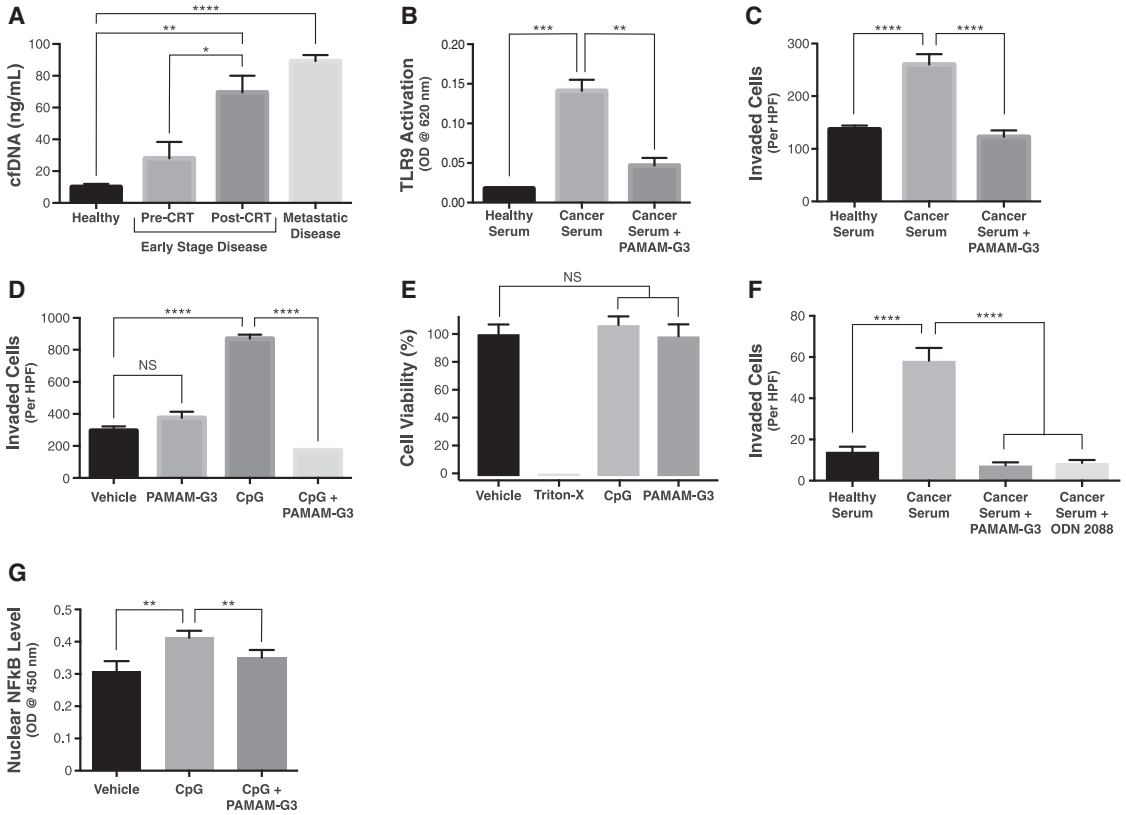

Figure 1. PAMAM-G3 Inhibits TLR-9-Activating, Pro-invasive DAMPs in Pancreatic Cancer

(A) Serum cfDNA levels in healthy individuals, PC patients with localized, early-stage disease before and after CRT, and PC patients with known metastatic disease (n = 8 for all groups). (B) Activation of TLR-9-specific reporter cells by either healthy human sera or PC patient sera in the absence or presence of PAMAM-G3 (20 μg/mL). (C) Invasion of Panc1 PC cells in a transwell-Matrigel assay after addition of either healthy human sera or PC patient sera in the absence or presence of PAMAM-G3 (20 μg/mL). (D) Invasion of Panc1 cells after treatment with vehicle (media) or the TLR-9-specific agonist CpG ODN 2006 (5 μM) in the absence or presence of PAMAM-G3 (20 μg/mL). Effect of PAMAM-G3 alone on Panc1 cell invasion is also shown. (E) Cell viability as measured by Cell-titer Glo luminescence assay was determined after incubation of Panc1 PC cells with vehicle (media), CpG ODN (5 μM), PAMAM-G3 (20 μg/mL), or 1% Triton X-100 for 24 hr. (F) Invasion of KPC4580P PC cells in a transwell-Matrigel assay after addition of either healthy human sera, PC patient sera, or PC patient sera in the presence of PAMAM-G3 (20 μg/mL) or the TLR 9 inhibitor ODN 2088. (G) Effect of vehicle (media) or CpG ODN 2006 (5 μM) treatment, alone or in combination with PAMAM-G3 (20 μg/mL), on nuclear translocation of NF-κB in BxPC3 PC cells. Bar graphs denote mean ± SEM. TLR 9 activation, PC cell invasion and viability, and NF-κB translocation experiments were repeated at least three times, and figures depict a single representative experiment. HPF, high powered field; RLU, relative light units. ****$p < 0.0001$; ***$p < 0.001$; **$p < 0.01$; *$p < 0.05$; and NS, not significant, by two-tailed t test.

However, most patients who undergo resection ultimately suffer recurrence with distant metastatic disease,[20] and the median survival of patients with metastatic disease is measured in months, even with aggressive chemotherapy.[21] The grave outcomes for PC patients justify the pursuit of more innovative therapeutic strategies.[22,23] Based on prior efficacy in non-cancerous disease models, we explored the ability of PAMAM-G3 to neutralize the downstream TLR-mediated and pro-invasive effects of extracellular nucleic acids and nucleic-acid-containing DAMPs in PC.

RESULTS

Nucleic-Acid-Containing DAMPs Are Elevated in PC Patients with Advanced Disease and Post-treatment

We first quantified levels of cell-free DNA (cfDNA) and associated DAMPs such as nucleosomes in the sera of PC patients. We found that PC patients with early stage (radiographically localized) disease have mildly elevated cfDNA levels compared to healthy volunteers, whereas patients with advanced stage or metastatic disease have dramatically higher cfDNA levels (Figure 1A). In order to further analyze the pattern of cfDNA release in patients with early stage disease during treatment, we collected sera at four time points: baseline (before any treatment), 4–6 weeks after the end of preoperative (neoadjuvant) chemoradiation therapy (CRT), intraoperatively during surgical resection, and 1 week postoperatively. We found that serum cfDNA and nucleosome levels were increased in response to CRT in our PC patient population, regardless of clinical response to therapy (Figures 1A and S1). Moreover, these markers were further elevated in the PC patients intraoperatively and to even a greater degree postoperatively (Figure S2).

NABP Inhibits TLR 9 Activating and Pro-invasive DAMPs from PC Patients

To determine whether PC patient sera contains DAMPs such as cfDNA and nucleic-acid-protein complexes that may stimulate the TLR family of receptors, we quantified activation of TLRs 9 and 4 in response to patient sera. Although TLR 9 recognizes unmethylated, CpG motif-bearing cfDNA species, TLR 4 can be activated by nucleosomes, and both of these types of DAMPs are known to circulate at elevated levels in other cancer and inflammatory disease states.[17,24–27] We observed that sera from PC patients induced significant activation of TLRs 9 and 4 as compared to normal sera (Figures 1B and S3). Addition of PAMAM-G3 significantly reduced stimulation of TLR 9 induced by the PC patient sera but not TLR 4 (Figures 1B and S3). These results suggest that nucleic acid DAMPs, such as cfDNA, present in PC patient sera induce TLR 9 activation in a manner that can be abrogated by PAMAM-G3.

Based on prior reports demonstrating that cfDNA/TLR 9 agonists can promote cancer cell invasion and metastasis,[8,9,15,28–30] we examined whether PC patient sera induces invasion of the Panc1 human PC cell line, which is known to express TLR 9, in a transwell-Matrigel assay.[31] Addition of PC patient sera, but not normal human sera, to Panc1 cells significantly increased their invasion, and this effect could be mitigated by administration of PAMAM-G3 (Figure 1C). To support the notion that the pro-invasive phenotype induced by PC patient sera may be nucleic acid/TLR 9 mediated, we confirmed that the TLR-9-specific agonist CpG oligonucleotide (ODN) 2006 also induced invasion of Panc1 cells, which was in turn inhibited by PAMAM-G3 (Figure 1D). Importantly, treatment with PAMAM-G3 by itself did not affect tumor cell invasion. In addition, neither CpG ODN nor PAMAM-G3 treatment alone influenced PC cell proliferation (Figures 1E and S4). Similar results were obtained with other human (BxPC3 and MiaPaCa2) or murine (KPC4580P) PC cell lines, all of which were known or found to express TLR 9 (Figure S5).

To further investigate whether the pro-invasive activity induced by PC patient sera is TLR 9 dependent, we performed similar PC cell invasion assays in the presence of the TLR-9-specific oligonucleotide inhibitor ODN 2088.[32] The TLR 9 inhibitor not only inhibited CpG ODN-mediated invasion of PC cells (Figure S6), it also inhibited cell invasion upon stimulation by PC patient sera as effectively as PAMAM-G3 (Figure 1F). These results are consistent with the notion that the neutralizing effects of PAMAM-G3 on PC patient sera-induced invasion are TLR 9 dependent.

To better understand the intracellular signaling mediating this TLR-9-mediated pro-invasive effect, we analyzed the activation of nuclear factor κB (NF-κB), a transcription factor and master regulator of the immune system that also contributes to tumor progression and metastasis in PC.[33] Upregulation of NF-κB-dependent transcriptional pathways is classically observed upon pro-inflammatory TLR activation.[34] Addition of CpG ODN to human BxPC3 and murine KPC4580P cells caused an increase in nuclear translocation of NF-κB, whereas co-treatment with PAMAM-G3 maintained nuclear NF-κB levels similarly to baseline (Figures 1F and S7A), suggesting that downstream activation of NF-κB in this manner may be responsible for the pro-invasive phenotype induced by TLR 9 ligation. Activation of other common TLR-dependent signaling pathways, such as the mitogen-activated protein kinase (MAPK)/extracellular signal-regulated kinase (ERK), Src, or STAT3 pathways,[35–40] was not observed in response to CpG treatment in these PC tumor cell lines (Figure S7B).

NABP Binds and Neutralizes Pro-invasive PC Microvesicles

Extracellular nucleic acids and nucleic acid complexes also circulate in or on lipid vesicles, including microparticles (MPs) and exosomes, and these vesicles are also known to potentiate tumor cell invasion and metastasis.[13,16,17,41,42] To determine if circulating microvesicles could also induce a similar pro-invasive effect, we isolated MPs from PC patient sera by differential centrifugation and tested their ability to stimulate Panc1 cell invasion. Both the vesicle-containing and vesicle-free fractions of PC patient sera contained notable cfDNA levels, confirming that cfDNA in PC patient sera is present in both vesicle-bound and unbound forms (Figure S8). Both serum fractions significantly promoted Panc1 cell invasion, effects that were in turn blocked by treatment with PAMAM-G3 (Figure 2A). These results indicate that PAMAM-G3 can neutralize pro-invasive nucleic-acid-containing DAMPs in PC patient sera in the form of free nucleic acids or nucleic-acid-protein complexes as well as microvesicles.

To our knowledge, a role for NABPs like PAMAM-G3 in modulating the activity of pro-invasive microvesicles has not been described before. To further investigate this observation, we assessed whether PAMAM-G3 can directly bind MPs isolated from PC patient sera. Assay plates pre-coated with PAMAM-G3 were incubated with varying concentrations of MPs, and microvesicle binding was quantified with a primary antibody recognizing a surface epitope. We found that PAMAM-G3 can directly bind MPs isolated from patient sera (Figure 2B) in a concentration-dependent manner. Analogously, we also demonstrated that PAMAM-G3 can bind tumor-derived MPs (Figure 2C) and exosomes (Figure 2D) harvested from cultured PC cells (KPC4580P) as well. Quantification of the zeta potential of MPs and exosomes secreted by KPC4580P cells showed that they bear a net electronegative surface charge, consistent with the presence of surface nucleic acids, as has been demonstrated for other cell-derived microvesicles,[16] as well as binding by PAMAM-G3 (Figure S9).

Based on prior studies showing that tumor-derived microvesicles can promote autocrine invasion of tumor cells in other cancer types,[41] we evaluated whether PC-derived microvesicles can also induce a similar pro-invasive phenotype and whether an NABP could mitigate this effect. In transwell-Matrigel invasion assays, addition of either MPs or exosomes (Figure 2E) harvested from cultured KPC4580P cells strongly induced tumor cell invasion in an autocrine fashion, and these effects were again significantly inhibited with PAMAM-G3 treatment. Neither addition of MPs nor exosomes alone influenced PC cell proliferation (Figure 2F). Thus, our findings suggest that

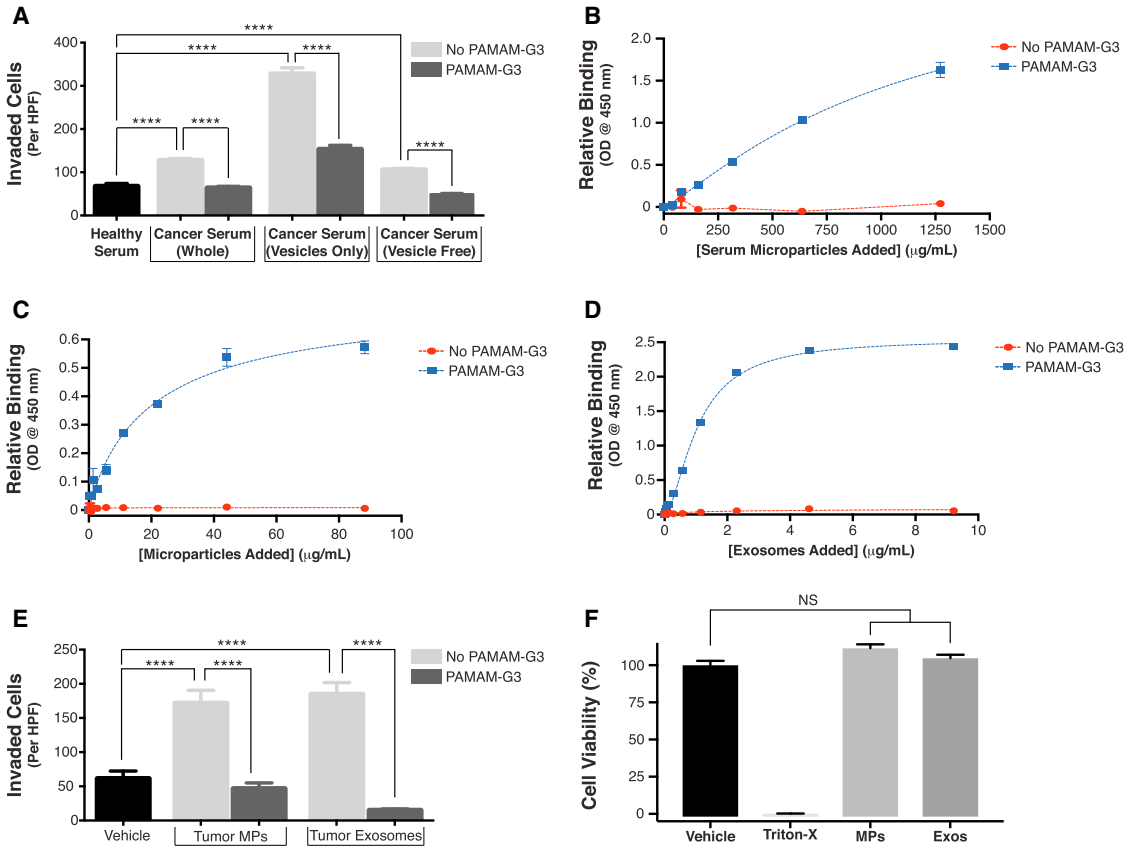

Figure 2. PAMAM-G3 Binds and Inhibits Pro-invasive Microvesicles Isolated from Both Pancreatic Cancer Patient Sera and Cell Lines

(A) PC patient sera were separated by centrifugation into MP-containing and MP-free fractions (supernatant). Quantification of Panc1 cell invasion in a transwell-Matrigel assay after addition of healthy human serum, whole PC patient serum, and each serum fraction in the absence or presence of PAMAM-G3 (20 μg/mL). (B–D) Concentration-dependent binding of MPs isolated from PC patient sera (B) as well as MPs (C) and exosomes (D) secreted by the KPC4580P PC cell line to assay plates coated without or with PAMAM-G3 (0.2 μg/mL), quantified using a custom-designed ELISA as described in the Materials and Methods section. (E) Invasion of KPC4580P cells after addition of KPC4580P-derived MPs (100 ng/μL) and exosomes (50 ng/μL), alone or in combination with PAMAM-G3 (20 μg/mL) or media (vehicle) in a transwell-Matrigel assay. (F) Cell viability as measured by Cell-titer Glo luminescence assay was determined after incubation of KPC4580P cells with vehicle (media), KPC4580P-derived MPs (100 ng/μL) or exosomes (exos, 50 ng/μL), or 1% Triton X-100 for 24 hr. Bar graphs depict mean ± SEM; all experiments were repeated at least three times, and figures depict a single representative experiment. HPF, high powered field; RLU, relative light units. ****$p < 0.0001$ by two-tailed t test.

PAMAM-G3 can neutralize the *in vitro* pro-invasive effects of both TLR-9-activating nucleic acid DAMPs and circulating microvesicles.

NABP Treatment Prevents Liver Metastasis and Reduces Levels of Pro-invasive DAMPs

Next, we sought to evaluate the therapeutic potential of PAMAM-G3 in a syngeneic immunocompetent murine model of PC metastasis. Established genetically engineered murine models (GEMM) of pancreatic adenocarcinoma such as the KPC model are poorly suited for studying experimental anti-metastatic therapies due to the limited occurrence of liver metastasis (~30%) and highly variable tumor growth in those mice.[43,44] For this reason, we established a syngeneic immunocompetent murine model of PC metastasis using the murine KPC4580P cell line, which is derived from the KPC GEMM model of PC[45] and bears the added benefit of constitutive luciferase expression, enabling quantitative measurement of tumor burden (Figure S10). In this model, C57BL/6 mice surgically implanted with 10^5 KPC4580P cells in their spleens reliably develop fulminant liver metastasis within 3 to 4 weeks. Because orthotopic implantation of PC tumor cells directly into the pancreas often does not yield consistent liver metastasis in murine models, as was also observed for the KPC4580P cell line, other investigators have used splenic injection to facilitate reproducible and timely liver metastasis.[43] Although this splenic implantation model of PC liver metastasis is limited by the fact that it only captures the final metastatic steps of tumor cell extravasation and colonization,[43] our *in vitro* studies demonstrating that PAMAM-G3 inhibits DAMP-induced invasion of PC tumor cells suggest that this model is suitable for investigating the polymer's effect on *in vivo* liver metastasis.

Groups of 25 mice were treated twice weekly with intraperitoneal injections of PAMAM-G3 (20 mg/kg; 10-fold below the maximum

tolerated dose as described elsewhere) or saline vehicle starting 48 hr after tumor cell implantation. Primary (spleen) and metastatic (liver) tumor burden were quantified by measuring tumor-specific *ex vivo* organ bioluminescence and weight after 3 weeks. As shown in Figures 3A and 3B, PAMAM-G3 treatment had no effect on primary tumor burden in the spleen. Remarkably, however, PAMAM-G3 treatment reduced liver metastatic burden by >90% ($p < 0.0001$) as measured by tumor cell bioluminescence (Figure 3A). Even more strikingly, the liver weights of PAMAM-G3-treated mice were normal and statistically equivalent to the weights of livers from healthy, age-matched tumor-free mice, whereas the liver weights of tumor-bearing mice not treated with the NABP increased by >70% ($p < 0.001$) (Figure 3B, left panel). In addition, the gross appearance of the livers from PAMAM-G3-treated mice was a stark contrast to the appearance of the livers from mice that did not receive the NABP, which were littered with metastatic disease (Figure 3B, right panel).

Because polycationic NABPs like PAMAM-G3 are primarily cleared by the liver,[46] we measured plasma levels of the aspartate aminotransferase (AST) and alanine aminotransferase (ALT) enzymes, which serve as biochemical markers of parenchymal damage (Figures 3C and 3D). We also looked for evidence of hepatic toxicity using two cohorts of mice that were healthy (tumor free), age-matched controls and treated with the same PAMAM-G3 or vehicle dosing scheme (20 mg/kg, twice weekly) and for the same duration (3 weeks) as the tumor-bearing mice. As shown in Figures 3C and 3D, vehicle-treated tumor-bearing mice displayed massive elevations in both AST and ALT compared to the vehicle-treated healthy controls, reflecting the large degree of hepatic dysfunction due to extensive tumor burden. In contrast, AST and ALT levels in tumor-bearing mice treated with PAMAM-G3 were significantly lower than their vehicle-treated counterparts and only mildly elevated compared to the healthy vehicle-treated controls. Importantly, no statistically significant increase in AST or ALT levels was detected in the cohort of healthy tumor-free mice given the same PAMAM-G3 regimen compared to those treated with vehicle, suggesting that PAMAM-G3 administration at the particular dosing scheme employed is not associated with liver injury. Likewise, considering that NABPs are secondarily cleared by the kidney,[46] no differences in renal function as measured by plasma creatinine and blood urea nitrogen (BUN) levels were observed between these two groups, further highlighting that PAMAM-G3 treatment demonstrated no evidence of clearance organ toxicity (Figures S11A and S11B).

Tumor-bearing mice treated with PAMAM-G3 also displayed improvements in other clinical measures that reflect systemic illness compared to those treated with vehicle. For example, although the tumor-bearing vehicle-treated group showed evidence of the hypoglycemia that is often clinically associated with hepatic failure due to extensive tumor burden, plasma glucose levels in the tumor-bearing PAMAM-G3-treated group were statistically unchanged from the healthy vehicle-treated controls (Figure 3E). Furthermore, platelet counts and hemoglobin levels were significantly decreased in the vehicle-treated tumor-bearing mice compared to the tumor-free controls, whereas levels of D-dimer (a fibrin degradation product) were significantly elevated (Figures 3F–3H). Taken together, these results are suggestive of acute clinical illness in the vehicle-treated tumor-bearing mice, leading to a disseminated intravascular coagulation (DIC)-like phenotype, which is consistent with the extensive tumor burden observed in these mice and the fact that PC cell lines are associated with high expression of the procoagulant tissue factor.[47] In contrast, the PAMAM-G3-treated tumor-bearing mice showed no evidence of thrombocytopenia or anemia compared to the healthy controls and only mildly elevated D-dimer levels. Beyond these systemic markers, the PAMAM-G3-treated PC mice were also visibly healthier than mice not given the NABP in qualitative measures, exhibiting normal activity and posture as well as positive response to stimulation. Moreover, no significant differences were observed between the healthy tumor-free mice treated with vehicle or PAMAM-G3 in regards to glucose, platelet, hemoglobin, albumin, or white blood cell levels (Figures 3E– 3G, S11C, and S11D), further underscoring the absence of any observed toxicity associated with PAMAM-G3 administration at the employed dosages.

Mice treated with PAMAM-G3 also showed significantly reduced levels of plasma cfDNA (Figure 4A), and cfDNA levels in all mice correlated with metastatic tumor burden (Figure 4B, $R^2 = 0.71$), but not primary tumor burden (Figure 4C, $R^2 = 0.05$). Moreover, mice treated with the NABP also displayed significantly lower levels of circulating nucleosomes and high mobility group box 1 (HMGB1) protein, which both represent pro-inflammatory nucleic acid associated DAMPs that have been implicated in promoting tumor invasion or metastasis[3,11,28,48] (Figures 4D and 4E). Importantly, pooled sera collected from vehicle-treated tumor-bearing mice triggered significantly more potent invasion of KPC4580P cells *in vitro* in comparison to sera isolated from mice treated with PAMAM-G3 or from healthy C57BL/6 controls (Figure 4F). Furthermore, exogenous addition of PAMAM-G3 to sera from vehicle-treated mice abrogated this pro-invasive effect on KPC4580P cells, reducing invasion levels similarly to those observed in the presence of sera from tumor-bearing mice treated with PAMAM-G3, but still higher than that seen with healthy mouse sera (Figure 4F). These findings support a proposed mechanism, wherein systemic administration of PAMAM-G3 in tumor-bearing mice may aid in neutralizing circulating factors, such as extracellular nucleic acids, nucleic-acid-protein complexes, and microvesicles, which promote tumor invasion and metastasis.

DISCUSSION

Here, we present the concept of using an NABP (PAMAM-G3) as a potential therapeutic to inhibit metastatic progression in PC. Our data indicate that cfDNA present in PC patient sera is a potent activator of TLR 9, which is expressed by PC cells and whose activation in the tumor stroma has been shown to potentiate PC metastasis *in vivo*.[7] The activation of TLR 9 leads to PC cell invasion *in vitro*, a critical step in tumor progression and metastasis. We observed that activation of TLR 9 by CpG ODN led to increased nuclear translocation of NF-κB, which has been associated with the expression of numerous pro-metastatic genes.[33] All of these pro-metastatic effects of TLR 9

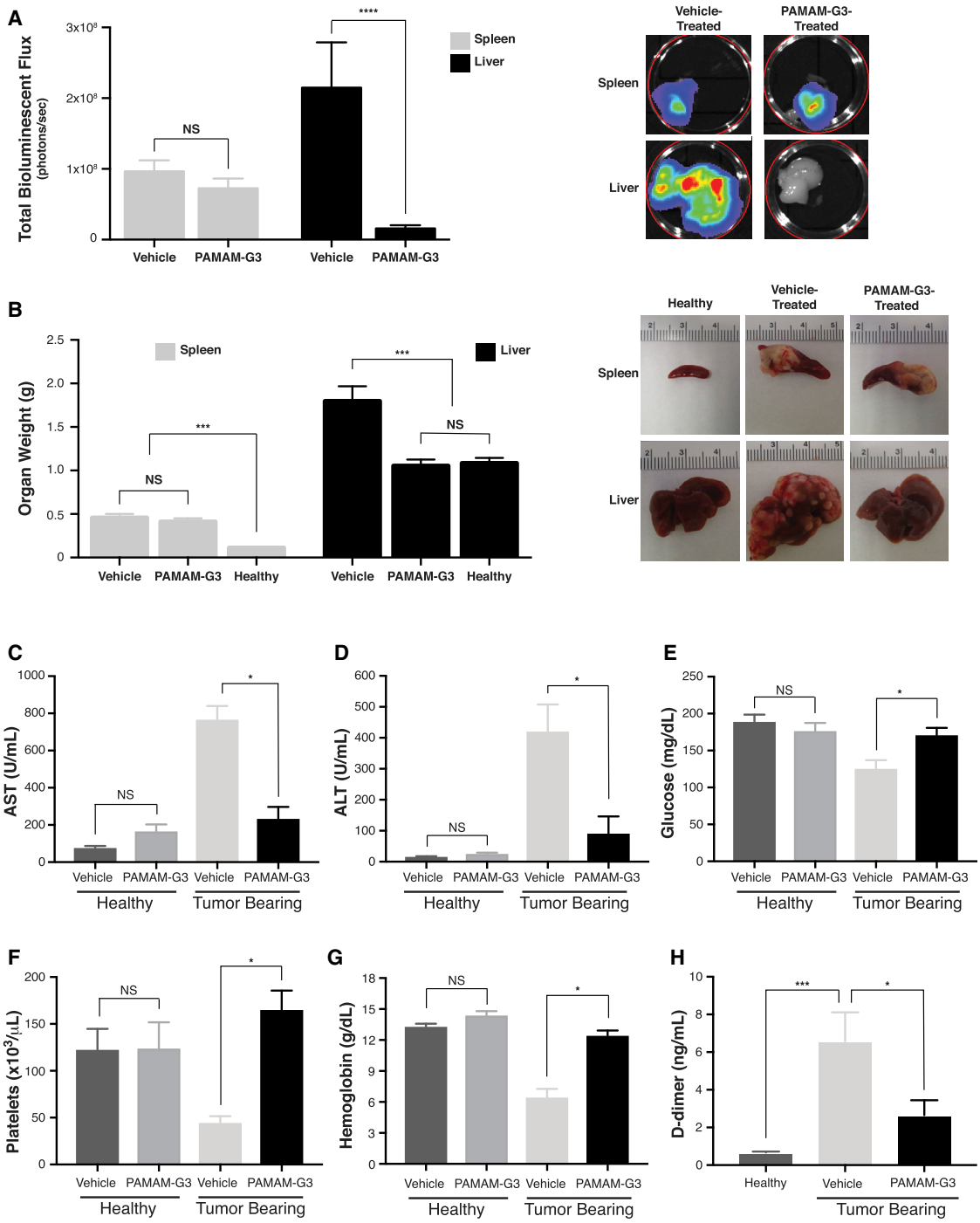

Figure 3. PAMAM-G3 Inhibits *In Vivo* Liver Metastasis without Affecting Primary Tumor Growth in a Syngeneic Murine Model of Pancreatic Cancer

(A and B) Quantification of primary (spleen) and metastatic (liver) tumor burden in vehicle (saline) or PAMAM-G3-treated KPC4580P tumor-bearing mice, as measured by both total organ bioluminescence (A, left panel) and gross organ weight (B, left panel). Figures depict cumulative data obtained from three individual tumor treatment studies for a total of n = 25 mice per group (vehicle or PAMAM-G3 treated). Representative images illustrate bioluminescent intensity (A, right panel) and gross appearance (B, right panel) of spleen and liver organs from mice treated with or without PAMAM-G3. Representative photographs and mean gross weights of spleen and liver organs from healthy C57BL6 control mice (n = 5) are also displayed. (C–H) Quantification of plasma AST (C), ALT (D), glucose (E), platelet (F), hemoglobin (G), and D-dimer (H) levels from tumor-bearing mice treated with vehicle or PAMAM-G3. AST, ALT, glucose, platelet, and hemoglobin levels measured in healthy tumor-free mice treated with vehicle (n = 10) or PAMAM-G3 (n = 9) are also illustrated. Bar graphs depict mean ± SEM. ****$p < 0.0001$; ***$p < 0.001$; *$p < 0.05$; and NS, not significant, by Kruskal-Wallis test.

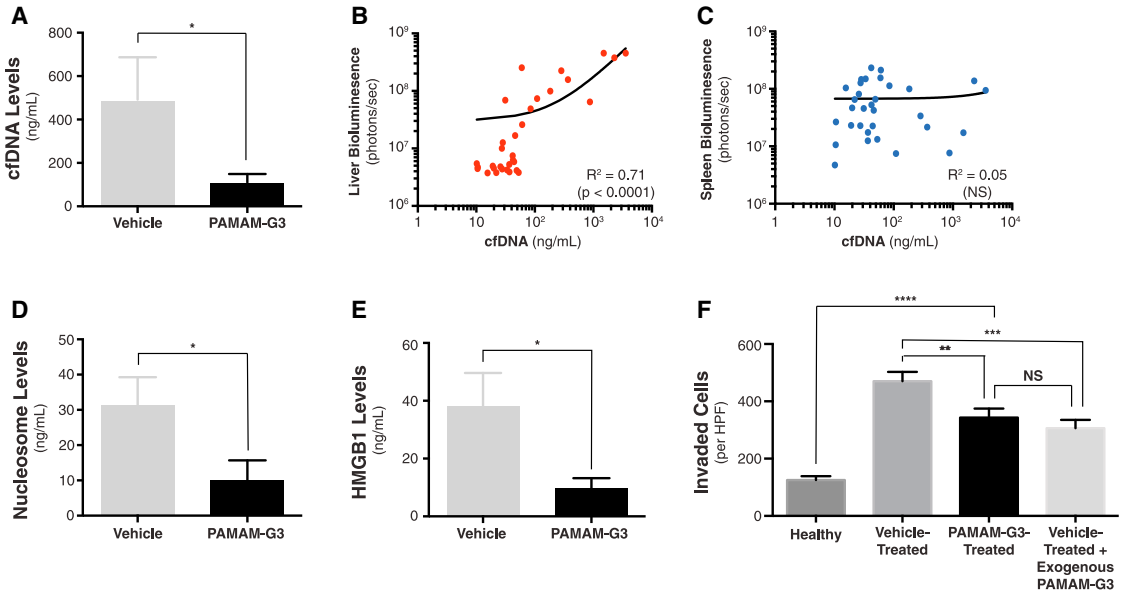

Figure 4. PAMAM-G3 Reduces Circulating Levels of Pro-invasive DAMPs in a Syngeneic Murine Model of Pancreatic Cancer

(A) Quantification of plasma cfDNA levels in KPC4580P tumor-bearing mice treated with vehicle or PAMAM-G3. Figure depicts cumulative data obtained from three individual tumor treatment studies for a total of n = 25 mice per group (vehicle or PAMAM-G3 treated). (B and C) Correlation between cfDNA levels and tumor burden in the liver (B) or spleen (C) in all mice. Data points in (B) and (C) reflect individual mice in the study. (D and E) Measurement of plasma nucleosome (D) and HMGB1 (E) levels in mice treated with or without PAMAM-G3. (F) *In vitro* transwell-Matrigel invasion of KPC4580P cells in the presence of pooled sera isolated from either healthy C57BL6 mice, PAMAM-G3-treated tumor-bearing mice, or vehicle-treated tumor-bearing mice, with or without exogenous PAMAM-G3 (20 μg/mL addition). Bar graphs depict mean ± SEM. ****p < 0.0001; ***p < 0.001; **p < 0.01; *p < 0.05; and NS, not significant, by two-tailed t test (A–F). cfDNA raw data in (A) were log-transformed in order to satisfy the normality requirement for parametric analysis by two-tailed t test.

activation are abrogated by PAMAM-G3 treatment *in vitro*. However, multiple redundant TLRs as well as non-TLR receptors exist that are activated by cfDNA, cfRNA, and associated proteins.[4] By directly neutralizing nucleic-acid-containing DAMPs upstream of these pathways, PAMAM-G3 can potentially inhibit this network.[2]

Our group has previously investigated the mechanism by which PAMAM-G3 neutralizes the downstream effects of TLR 9 agonists such as CpG ODN.[2] We observed that PAMAM-G3 inhibits the functional activity of B-type CpG ODN by both decreasing its cellular uptake and re-localizing the fraction that is taken up by cells from the endosomal compartment to the nucleus, thereby preventing its subsequent interaction with TLR 9.[2] We expect that these multifaceted actions underlie the ability of PAMAM-G3 to inhibit nucleic acid DAMP-induced PC cell invasion *in vitro* and PC metastasis *in vivo*, as observed in the present study.

Extracellular nucleic acids and nucleic acid complexes also circulate in or on lipid microvesicles. These particles can potentiate metastasis by acting on tumor cells directly as well as pre-conditioning the pre-metastatic site for tumor implantation.[13,14,41] Our data show that these particles have a net electronegative charge, presumably due to the presence of negatively charged nucleic acids on the vesicle surface as other studies have demonstrated,[16] allowing for direct binding by an NABP-like PAMAM-G3. Furthermore, we show that PAMAM-G3 can neutralize the pro-invasive effects of microparticles and exosomes on tumor cells in culture. Thus, NABPs also represent a useful tool for studying and modulating the pro-metastatic effects of microvesicles.

The inhibitory effects of NABPs on PC *in vitro* motivated us to study them in a syngeneic immunocompetent murine model of PC metastasis. By utilizing the bioluminescent KPC4580P cell line derived from the clinically relevant KPC genetically engineered murine model of pancreatic adenocarcinoma, this model captures the critical genetic hallmarks of human PC disease. Likewise, splenic implantation of the PC cells facilitates a robust and reliable metastatic time course, making the model well-suited for assessing the efficacy of a potential anti-metastatic therapeutic strategy.[44] We found that PAMAM-G3-treated mice had dramatically less metastatic disease in the liver than vehicle-control-treated mice. The therapeutic benefit of PAMAM-G3 administration was not only reflected by the quantifiable reduction in tumor burden, but also by substantial improvements in plasma indicators of liver damage and other clinical markers of illness. However, PAMAM-G3 therapy did not significantly affect primary tumor growth in the spleen, suggesting that its effect targets the metastatic process and not proliferation, consistent with our *in vitro* observations. Despite the limitation that our model does not fully recapitulate the natural course of PC metastasis on account of splenic implantation of the PC cells, our model successfully

captures the final metastatic steps of tumor cell extravasation and colonization. In this light, we believe that NABPs may represent an innovative anti-metastatic therapy. Our observations are also consistent with studies demonstrating that extracellular DNA and DNA-protein complexes promote cancer progression[9,15,28,29,49–51] and that DNase I treatment can reduce metastasis in other tumor models.[9,15,29] However, our findings also suggest that using an NABP to target circulating nucleic acids and associated complexes that facilitate metastasis may offer the added and important benefit of neutralizing pro-metastatic contributions of tumor-derived microvesicles, which may potentiate its robust anti-metastatic therapeutic response *in vivo*.[15,29]

PC is a devastating disease, largely due to its aggressively metastatic nature. Neoadjuvant (preoperative) and adjuvant (postoperative) therapy with chemotherapy and with or without radiation therapy are often given to patients with localized disease, with the goal of eradicating micrometastatic disease.[52] However, even with aggressive preoperative and postoperative therapy, most patients ultimately develop and succumb to metastatic disease. Studies have also demonstrated that tumor manipulation during surgical resection may result in the release of circulating tumor cells in colorectal and lung cancers.[9,53] Our data suggest that two of the treatments we use for treatment of localized disease (chemoradiation therapy and surgical resection) may lead to increased levels of circulating DAMPs that, in turn, promote metastatic disease. Unfortunately, the treatments we are using to try to cure patients with PC may predispose them to distant metastasis. NABPs could be combined with standard treatment regimens to inhibit the effects of treatment-induced DAMPs. For example, NABP treatment could be initiated with neoadjuvant therapy and/or prior to surgical resection, potentially decreasing the risk of distant metastasis and increasing the proportion of patients who are cured. The anti-thrombotic effects of NABPs that we have previously observed could be an important secondary benefit in this population at high-risk for thrombotic complications.[54,55] Despite many improvements in the treatment of PC, we have made little impact on the cure rate. Thus, NABPs represent an inventive approach to modulate the tumor microenvironment and potentially reduce metastasis in patients with localized PC. Moreover, because certain NABPs have already been evaluated clinically as vehicles for small interfering RNA (siRNA) delivery in cancer patients, with minimal evidence of toxicity, a precedent exists for safely translating these agents to the bedside, albeit not without pre-assembling the NABP into a nucleic-acid-containing complex.[56] Thus, given the major unmet need for therapies that limit metastasis, particularly in PC, we believe that clinical development of this NABP-based approach is feasible.

Although concerns regarding the safety and clinical use of NABPs like PAMAM-G3 have been raised,[46] the work presented here, together with prior studies by our group and others in the literature, may serve to alleviate some of these reservations. For example, although it is known that polycationic dendrimers such as PAMAM-G3 are primarily cleared by the liver and kidney and can be toxic to these organs,[46] the toxicity of these polymers is dosage dependent and the maximum tolerated *in vivo* doses of PAMAM-G3 in prior murine studies were reportedly up to 1,000 mg/kg, 50 times higher than the efficacious dose used in our current study and previous studies in other disease models.[5,46,57] Thus, the dosages of PAMAM-G3 needed to inhibit metastatic spread in the presented model of PC are well within the limits of the maximally tolerated dose. Furthermore, herein we show that healthy non-tumor-bearing mice treated with the same PAMAM-G3 dosing scheme displayed no laboratory abnormalities in hepatic or renal function or other common clinical markers over the duration of the study, suggesting that the NABP was well-tolerated. These results highlight that an NABP-based therapeutic strategy can be safely administered at doses that may prove clinically efficacious.

Although the results of the study provide an encouraging proof of concept demonstrating the potential value of an NABP as an agent for combating metastatic disease in a cancer model, it will be informative to explore the generalized therapeutic utility of NABPs in other inflammatory cancer types, including breast cancer or soft tissue sarcoma. Moreover, future work should also aim to exploit the binding properties of an NABP-like PAMAM-G3 that enable it to capture an array of circulating bioactive molecules. Characterizing the diversity and composition of these extracellular DAMPs or microvesicles will aid in developing a more thorough systems-biology-driven understanding of tumor progression and metastasis *in vivo*. Because an NABP-based strategy inhibits multiple pro-metastatic pathways, elucidating a complete mechanistic understanding of the agent's *in vivo* actions is challenging, but this property may in fact represent a therapeutic advantage, given the ease with which tumors evolve drug resistance to treatments that target only a single pathway. In addition, although we selected a well-characterized NABP for these initial studies, we recognize that PAMAM-G3 and other established NABPs were not originally identified on the basis of their ability to bind and neutralize extracellular nucleic acids and microvesicles that play a pathological role in cancer. Thus, we believe the findings of this study present an opportunity for exploiting existing polymer screening libraries[58–60] to identify novel NABPs that may have enhanced efficacy for treating cancer.

MATERIALS AND METHODS

Patient Blood Collection

With approval from the Duke University Institutional Review Board, blood was collected from patients with PC after presentation with localized (early stage) or advanced disease and—in those patients with early stage disease—at various time points in their treatment course, including before and after neoadjuvant (preoperative) chemoradiation therapy, intraoperatively during surgical resection immediately post-Kocher maneuver, and 1 week postoperatively. Neoadjuvant chemoradiation therapy consisted of 45–50 Gy of external beam radiation therapy delivered over approximately 5 weeks with concurrent oral capecitabine as a radiation sensitizer.[61] Patients

with advanced disease had undergone a variety of therapies, including chemotherapy and/or radiation therapy.

Reagents

Generation 3.0 polyamidoamine dendrimer solution (PAMAM-G3) was purchased from Sigma Aldrich (Cat. # 412422). The TLR agonists CpG ODN 2006, CpG ODN 1826, ODN 2088, Poly I:C, lipopolysaccharide (LPS), and R848 were purchased from Invivogen.

PC Cell Lines

Human BxPC3, Panc1, MiaPaCa2, and AsPc1 PC cell lines were purchased from ATCC. The luciferase-expressing KPC4580P murine PC cell line, derived from the KPC genetic mouse model of pancreatic ductal adenocarcinoma (a gift of Jen Jen Yeh, MD), was generated as described in the Supplemental Materials and Methods, along with information regarding growth media for all cell lines used.

Quantification of Cell-free DNA, Nucleosome, and HMGB1 Levels

Total DNA was isolated from sera using the DNA Blood Mini Kit (QIAGEN) and quantified using the PicoGreen Staining Kit (Life Technologies). Nucleosome levels were quantified using the Cell Death ELISA Plus Kit (Roche). HMGB1 levels were quantified using an ELISA kit (Chondrex).

TLR Activation Assays

HEK-Blue TLR 4 and 9 reporter cell lines were purchased from Invivogen, and activation in response to control agonists or human sera was determined according to the manufacturer's instructions. These cells stably co-express a TLR gene and an NF-κB-inducible SEAP (secreted embryonic alkaline phosphatase) reporter gene that can be monitored using SEAP detection media. Additional details are provided in the Supplemental Materials and Methods. Briefly, these cells were plated in 96-well plates at a density of 100,000 cells per well and treated for 18–24 hours with either (1) media alone, (2) a control agonist for each given TLR (LPS [1 μg/mL] for TLR 4 and CpG ODN [5 μM] for TLR 9), (3) cancer patient sera (3.5 μL), (4) normal human sera (3.5 μL), (5) media + PAMAM-G3 (20 μg/mL), (6) control agonist + PAMAM-G3 (20 μg/mL), (7) cancer patient sera (3.5 μL) + PAMAM-G3 (20 μg/mL), or (8) normal patient sera (3.5 μL) + PAMAM-G3 in a final volume of 100 μL. The cell supernatant was subsequently collected and mixed with Quantiblue (Invivogen) at a 60:40 v:v ratio and incubated for 5 hr at 37°C, after which time absorbance at 650 nm was measured using a Spectramax i3 plate reader (Molecular Devices).

Microparticle and Exosome Isolation from Cultured PC Cell Lines and PC Patient Sera

Further details are provided in the Supplemental Materials and Methods. Briefly, KPC-4580P cells were cultured to confluence, at which time media was replaced with complete medium supplemented with exosome-depleted FBS. After 72 hr, the supernatant was collected and centrifuged at 4,000 × *g* for 5 min to deplete cell debris. The residual supernatant was centrifuged at 20,000 × *g* for 20 min at 4°C to pellet MPs. The supernatant was removed and saved for exosome isolation. The MP pellet was washed once with PBS (−/−) before collection and resuspension in PBS. The supernatant from the initial MP spin was centrifuged at 100,000 × *g* for 2 hr at 4°C to pellet exosomes. After discarding the supernatant, the exosome pellet was washed once with PBS before collection and resuspension in PBS. The protein concentration of the MPs and exosomes was quantified via Pierce BCA assay (Thermo Fisher Scientific). To isolate MPs from human sera, sera was similarly centrifuged at 20,000 × *g* for 20 min at 4°C, washed, and resuspended in PBS.

Transwell-Matrigel Invasion Chamber Assays

Transwell-Matrigel invasion chambers were purchased from Corning and assays were performed according to the manufacturer's instructions. Briefly, the invasion chambers were first incubated with serum-free media in the top and bottom chambers at 37°C to allow the Matrigel to solidify and the two chambers to equilibrate in preparation for the addition of PC cells and various agonists and/or inhibitors, such as CpG ODN, PC-cell-line-derived MPs and exosomes, PAMAM-G3, or ODN 2088. The human (BxPC3, MiaPaca2, PANC-1, and AsPC-1) or mouse (KPC-4580P) PC cell lines were trypsinized, resuspended, and diluted in serum-free media. After aspiration of media from both chambers, cells were plated in the top chamber at a density of 50,000 cells/well (500-μL final volume) in the presence of serum-free media alone or various combinations of agonists and/or PAMAM-G3 (20 μg/mL) or ODN 2088 (100 μM). Agonists tested included CpG ODN (5 μM), PC-cell-line-derived MPs or exosomes (isolated as described above), PC patient sera or normal human sera (50 μL), or mouse sera (45 μL). 750 μL of complete media was added to the bottom chambers. The plated invasion chambers were incubated at 37°C for 24 hr, after which time media was aspirated from the top chambers. The top chambers were then removed and treated with 10% formaldehyde to fix the invaded cells on the bottom surface of the chamber, washed with PBS, and stained with crystal violet solution (5% w/v crystal violet, 25% v/v methanol). The chambers were then washed thoroughly in deionized water, and membranes were imaged using an inverted light microscope (Olympus IX50) at 4X magnification. 10 random images of each membrane were taken using an eyepiece camera (Dino-Eye AM7023B). The cells in the images were then counted using an ImageJ algorithm unique for each cell line (http://imagej.net/Particle_Analysis). Additional details are provided in the Supplemental Materials and Methods.

Analysis of Nuclear NF-κB Translocation

KPC-4580P cells (2×10^6 cells per plate) and BxPC3 cells (2×10^5 cells per plate) were seeded in 35-mm plates overnight. The cells were then treated with serum-free media alone, CpG ODN (1826 or 2006) (5 μM), or CpG (5 μM) and PAMAM-G3 (20 μg/mL) for 1 hr. Cell nuclei were then isolated using a nuclear isolation kit (Active Motif) using the manufacturer's guidelines. The protein content of each nuclear extract was quantified and standardized using a Protein Quantification Kit (Active Motif). The nuclear extract was then used to quantify nuclear translocation of NF-κB via ELISA. For the murine

nuclear extracts, nuclear translocation of p50 NF-κB was quantified using the Pierce p50 Transcription Factor Assay Kit (Thermo Fisher Scientific) using the manufacturer's instructions. For the human nuclear extracts, nuclear translocation of p65 NF-κB was quantified using the p65 TransAM ELISA (Active Motif).

Analysis of Cell Viability

In order to replicate conditions used for the invasion chamber assays, Panc1 or KPC4580P cells were seeded overnight in 96-well assay plates at a density of 50,000 cells/well. Panc1 cells were then treated with CpG ODN 2006 (5 μM), PAMAM-G3 (20 μg/mL), 1% Triton X-100, or media (12 wells per treatment group). After 24 hr, cell viability was measured according to the Cell Titer Glo Luminescent Cell Viability Assay (Promega) according to the manufacturer's instructions. KPC4580P cells were treated with CpG ODN 1826 (5 μM), KPC4580P-derived MPs (100 ng/μL), KPC4580P-derived exosomes (50 ng/μL), PAMAM-G3 (20 μg/mL), or media (4 wells per treatment group). After 24 hr, cell viability was measured according to the Cell Titer Glo Luminescent Cell Viability Assay (Promega) according to the manufacturer's instructions.

ELISA for Detection of PAMAM-G3 Binding to MPs

The binding of MPs and exosomes to PAMAM-G3 was quantified using a custom-designed ELISA assay and is described in detail in the Supplemental Materials and Methods. MPs and exosomes were isolated from KPC4580P PC cell cultures as described above. 96-well high-binding, flat-bottom plates (Corning) were coated overnight at 4°C with PAMAM-G3 diluted into PBS (−/−) at varying concentrations. After the wells were washed with PBS, incubated for 2 hr at room temperature (RT) with blocking buffer (PBS plus 5% BSA and 0.05% Tween 20), and washed again with PBS, the wells were incubated with varying concentrations of MPs or exosomes for 2 hr at RT. After a subsequent washing step, the wells were then incubated with either the polyclonal goat immunoglobulin G (IgG) against murine tissue factor (AF3178, R&D Systems) for MP detection or the monoclonal mouse IgG antibody against phosphatidylserine (05-719, Millipore) for exosome detection, followed by washing and detection using a horseradish-peroxidase-conjugated secondary antibody, and finally quantification of absorbance at 450 nm after TMB substrate addition. The binding of PC patient-derived MPs to PAMAM was quantified analogously.

Syngeneic Murine Model of PC Metastasis

All animal experiments were performed in compliance with Duke Institutional Animal Care and Use Committee (IACUC) protocols. Briefly, for the metastasis studies, KPC4580P luciferase expressing, murine PC cells (described above) were surgically implanted into the spleens of 12-week-old female C57BL6 mice. Starting on day 2 after tumor cell implantation, mice were treated twice per week with either intraperitoneal PAMAM-G3 (20 mg/kg) or saline for 3 weeks or until humane endpoints were reached, at which time the mice were sacrificed. Liver and spleen were harvested from each mouse for assessment of gross organ weight and *ex vivo* quantification of bioluminescent intensity (IVIS Kinetic). Just prior to sacrifice, caudal vena cava blood was collected from each mouse for analysis of blood cell counts (Heska HemaTrue blood analyzer), plasma cfDNA (described above), nucleosome levels (described above), HMGB1 levels (described above), or chemistry (performed by Duke DLAR Veterinary Diagnostic Laboratory) or for serum invasion assays (described above). Detailed description of the tumor cell implantation procedure is provided in the Supplemental Materials and Methods. For PAMAM-G3 toxicity studies, 12-week-old female C57BL6 mice were treated twice per week with either intraperitoneal PAMAM-G3 (20 mg/kg) or saline for 3 weeks, at which time the mice were sacrificed. Just prior to sacrifice, submandibular blood was collected from each mouse for blood cell count analysis or plasma chemistry analysis as described above.

Statistical Analysis

All data were plotted and analyzed using GraphPad Prism or JMP software. Data were all tested for normality prior to statistical analyses. If normally distributed, differences between groups were compared using a two-tailed Student's t test. If the data were not normally distributed, as in the case of the *in vivo* organ bioluminescence and gross weight data, statistical analysis between groups was performed using the Kruskal Wallis test.

SUPPLEMENTAL INFORMATION

Supplemental Information includes Supplemental Materials and Methods and eleven figures and can be found with this article online at https://doi.org/10.1016/j.ymthe.2018.02.018.

AUTHOR CONTRIBUTIONS

I.N., R.G., R.R.W., and B.A.S. designed the experiments. I.N., R.G., J.E.M., A.M., R.E.R., and D.C.R. performed the experiments. S.G.H. generated the KPC4580P cell line. I.N., R.G., D.S.P., J.L., R.R.W., and B.A.S. interpreted the data. I.N., R.G., R.R.W., and B.A.S. wrote the manuscript.

CONFLICTS OF INTEREST

Duke University has applied for a patent on this strategy to limit cancer progression.

ACKNOWLEDGMENTS

This work was supported in part by the Elsa Pardee Foundation (to R.R.W.), Department of Defense (DoD) Breast Cancer Research Program (BCRP) award W81WH-16-1-0513 (to B.A.S.), and NIH grants F30HL127977 (to R.G.), T32 GM007171 (to R.G. and I.N.), R01HL065222 (to B.A.S.), and U19AI067798 (to B.A.S.). We also acknowledge Duke Cancer Institute grant P30-CA014236 for support of the in vivo imaging facility. We would also like to acknowledge Jen Jen Yeh, MD, for her help with acquiring the KPC4580P cell line, the Duke DLAR Veterinary Diagnostic Lab for assistance with murine plasma chemistry analysis, Duke Cancer Institute grant P30-CA014236 for support of the Duke Optical Molecular Imaging and Analysis facility, and George Pitoc, Eda Holl, and Smita Nair for useful discussion.

REFERENCES

1. Morille, M., Passirani, C., Vonarbourg, A., Clavreul, A., and Benoit, J.-P.P. (2008). Progress in developing cationic vectors for non-viral systemic gene therapy against cancer. Biomaterials *29*, 3477–3496.
2. Lee, J., Sohn, J.W., Zhang, Y., Leong, K.W., Pisetsky, D., and Sullenger, B.A. (2011). Nucleic acid-binding polymers as anti-inflammatory agents. Proc. Natl. Acad. Sci. USA *108*, 14055–14060.
3. Pisetsky, D.S. (2012). The origin and properties of extracellular DNA: from PAMP to DAMP. Clin. Immunol. *144*, 32–40.
4. Kawasaki, T., Kawai, T., and Akira, S. (2011). Recognition of nucleic acids by pattern-recognition receptors and its relevance in autoimmunity. Immunol. Rev. *243*, 61–73.
5. Holl, E.K., Shumansky, K.L., Borst, L.B., Burnette, A.D., Sample, C.J., Ramsburg, E.A., and Sullenger, B.A. (2016). Scavenging nucleic acid debris to combat autoimmunity and infectious disease. Proc. Natl. Acad. Sci. USA *113*, 9728–9733.
6. Harmey, J.H., Bucana, C.D., Lu, W., Byrne, A.M., McDonnell, S., Lynch, C., Bouchier-Hayes, D., and Dong, Z. (2002). Lipopolysaccharide-induced metastatic growth is associated with increased angiogenesis, vascular permeability and tumor cell invasion. Int. J. Cancer *101*, 415–422.
7. Zambirinis, C.P., Levie, E., Nguy, S., Avanzi, A., Barilla, R., Xu, Y., Seifert, L., Daley, D., Greco, S.H., Deutsch, M., et al. (2015). TLR9 ligation in pancreatic stellate cells promotes tumorigenesis. J. Exp. Med. *212*, 2077–2094.
8. Ilvesaro, J.M., Merrell, M.A., Li, L., Wakchoure, S., Graves, D., Brooks, S., Rahko, E., Jukkola-Vuorinen, A., Vuopala, K.S., Harris, K.W., and Selander, K.S. (2008). Toll-like receptor 9 mediates CpG oligonucleotide-induced cellular invasion. Mol. Cancer Res. *6*, 1534–1543.
9. Tohme, S., Yazdani, H.O., Al-Khafaji, A.B., Chidi, A.P., Loughran, P., Mowen, K., Wang, Y., Simmons, R.L., Huang, H., and Tsung, A. (2016). Neutrophil extracellular traps promote the development and progression of liver metastases after surgical stress. Cancer Res. *76*, 1367–1380.
10. Schwarzenbach, H., Hoon, D.S.B., and Pantel, K. (2011). Cell-free nucleic acids as biomarkers in cancer patients. Nat. Rev. Cancer *11*, 426–437.
11. Holdenrieder, S., Nagel, D., Schalhorn, A., Heinemann, V., Wilkowski, R., von Pawel, J., Raith, H., Feldmann, K., Kremer, A.E., Müller, S., et al. (2008). Clinical relevance of circulating nucleosomes in cancer. Ann. N Y Acad. Sci. *1137*, 180–189.
12. Diaz, L.A., Jr., and Bardelli, A. (2014). Liquid biopsies: genotyping circulating tumor DNA. J. Clin. Oncol. *32*, 579–586.
13. Costa-Silva, B., Aiello, N.M., Ocean, A.J., Singh, S., Zhang, H., Thakur, B.K., Becker, A., Hoshino, A., Mark, M.T., Molina, H., et al. (2015). Pancreatic cancer exosomes initiate pre-metastatic niche formation in the liver. Nat. Cell Biol. *17*, 816–826.
14. Janowska-Wieczorek, A., Wysoczynski, M., Kijowski, J., Marquez-Curtis, L., Machalinski, B., Ratajczak, J., and Ratajczak, M.Z. (2005). Microvesicles derived from activated platelets induce metastasis and angiogenesis in lung cancer. Int. J. Cancer *113*, 752–760.
15. Wen, F., Shen, A., Choi, A., Gerner, E.W., and Shi, J. (2013). Extracellular DNA in pancreatic cancer promotes cell invasion and metastasis. Cancer Res. *73*, 4256–4266.
16. Ullal, A.J., Reich, C.F., 3rd, Clowse, M., Criscione-Schreiber, L.G., Tochacek, M., Monestier, M., and Pisetsky, D.S. (2011). Microparticles as antigenic targets of antibodies to DNA and nucleosomes in systemic lupus erythematosus. J. Autoimmun. *36*, 173–180.
17. Thierry, A.R., El Messaoudi, S., Gahan, P.B., Anker, P., and Stroun, M. (2016). Origins, structures, and functions of circulating DNA in oncology. Cancer Metastasis Rev. *35*, 347–376.
18. Varghese, A.M., Lowery, M.A., Yu, K.H., and O'Reilly, E.M. (2016). Current management and future directions in metastatic pancreatic adenocarcinoma. Cancer *122*, 3765–3775.
19. Siegel, R.L., Miller, K.D., and Jemal, A. (2016). Cancer statistics, 2016. CA Cancer J. Clin. *66*, 7–30.
20. Oettle, H., Neuhaus, P., Hochhaus, A., Hartmann, J.T., Gellert, K., Ridwelski, K., Niedergethmann, M., Zülke, C., Fahlke, J., Arning, M.B., et al. (2013). Adjuvant chemotherapy with gemcitabine and long-term outcomes among patients with resected pancreatic cancer: the CONKO-001 randomized trial. JAMA *310*, 1473–1481.
21. Von Hoff, D.D., Ervin, T., Arena, F.P., Chiorean, E.G., Infante, J., Moore, M., Seay, T., Tjulandin, S.A., Ma, W.W., Saleh, M.N., et al. (2013). Increased survival in pancreatic cancer with nab-paclitaxel plus gemcitabine. N. Engl. J. Med. *369*, 1691–1703.
22. Tuveson, D.A., and Neoptolemos, J.P. (2012). Understanding metastasis in pancreatic cancer: a call for new clinical approaches. Cell *148*, 21–23.
23. Varadhachary, G.R., and Wolff, R.A. (2016). Current and evolving therapies for metastatic pancreatic cancer: are we stuck with cytotoxic chemotherapy? J. Oncol. Pract. *12*, 797–805.
24. Marsman, G., Zeerleder, S., and Luken, B.M. (2016). Extracellular histones, cell-free DNA, or nucleosomes: differences in immunostimulation. Cell Death Dis. *7*, e2518.
25. Berger, R., Fiegl, H., Goebel, G., Obexer, P., Ausserlechner, M., Doppler, W., Hauser-Kronberger, C., Reitsamer, R., Egle, D., Reimer, D., et al. (2010). Toll-like receptor 9 expression in breast and ovarian cancer is associated with poorly differentiated tumors. Cancer Sci. *101*, 1059–1066.
26. Tian, J., Avalos, A.M., Mao, S.Y., Chen, B., Senthil, K., Wu, H., Parroche, P., Drabic, S., Golenbock, D., Sirois, C., et al. (2007). Toll-like receptor 9-dependent activation by DNA-containing immune complexes is mediated by HMGB1 and RAGE. Nat. Immunol. *8*, 487–496.
27. Yuan, Y., Yang, M., Wang, K., Sun, J., Song, L., Diao, X., Jiang, Z., Cheng, G., and Wang, X. (2017). Excessive activation of the TLR9/TGF-β1/PDGF-B pathway in the peripheral blood of patients with systemic lupus erythematosus. Arthritis Res. Ther. *19*, 70.
28. Liu, Y., Yan, W., Tohme, S., Chen, M., Fu, Y., Tian, D., Lotze, M., Tang, D., and Tsung, A. (2015). Hypoxia induced HMGB1 and mitochondrial DNA interactions mediate tumor growth in hepatocellular carcinoma through Toll-like receptor 9. J. Hepatol. *63*, 114–121.
29. Park, J., Wysocki, R.W., Amoozgar, Z., Maiorino, L., Fein, M.R., Jorns, J., Schott, A.F., Kinugasa-Katayama, Y., Lee, Y., Won, N.H., et al. (2016). Cancer cells induce metastasis-supporting neutrophil extracellular DNA traps. Sci. Transl. Med. *8*, 361ra138.
30. Merrell, M.A., Ilvesaro, J.M., Lehtonen, N., Sorsa, T., Gehrs, B., Rosenthal, E., Chen, D., Shackley, B., Harris, K.W., and Selander, K.S. (2006). Toll-like receptor 9 agonists promote cellular invasion by increasing matrix metalloproteinase activity. Mol. Cancer Res. *4*, 437–447.
31. Wu, H.Q., Wang, B., Zhu, S.K., Tian, Y., Zhang, J.H., and Wu, H.S. (2011). Effects of CPG ODN on biological behavior of PANC-1 and expression of TLR9 in pancreatic cancer. World J. Gastroenterol. *17*, 996–1003.
32. Stunz, L.L., Lenert, P., Peckham, D., Yi, A.K., Haxhinasto, S., Chang, M., Krieg, A.M., and Ashman, R.F. (2002). Inhibitory oligonucleotides specifically block effects of stimulatory CpG oligonucleotides in B cells. Eur. J. Immunol. *32*, 1212–1222.
33. Prabhu, L., Mundade, R., Korc, M., Loehrer, P.J., and Lu, T. (2014). Critical role of NF-κB in pancreatic cancer. Oncotarget *5*, 10969–10975.
34. Kawai, T., and Akira, S. (2007). Signaling to NF-kappaB by Toll-like receptors. Trends Mol. Med. *13*, 460–469.
35. Rakoff-Nahoum, S., and Medzhitov, R. (2009). Toll-like receptors and cancer. Nat. Rev. Cancer *9*, 57–63.
36. Kawai, T., and Akira, S. (2005). Toll-like receptor downstream signaling. Arthritis Res. Ther. *7*, 12–19.
37. Grivennikov, S.I., and Karin, M. (2010). Dangerous liaisons: STAT3 and NF-kappaB collaboration and crosstalk in cancer. Cytokine Growth Factor Rev. *21*, 11–19.
38. Yu, H., Pardoll, D., and Jove, R. (2009). STATs in cancer inflammation and immunity: a leading role for STAT3. Nat. Rev. Cancer *9*, 798–809.
39. Lowell, C.A. (2011). Src-family and Syk kinases in activating and inhibitory pathways in innate immune cells: signaling cross talk. Cold Spring Harb. Perspect. Biol. *3*, 3.
40. Wagner, E.F., and Nebreda, A.R. (2009). Signal integration by JNK and p38 MAPK pathways in cancer development. Nat. Rev. Cancer *9*, 537–549.
41. Menck, K., Scharf, C., Bleckmann, A., Dyck, L., Rost, U., Wenzel, D., Dhople, V.M., Siam, L., Pukrop, T., Binder, C., and Klemm, F. (2015). Tumor-derived microvesicles mediate human breast cancer invasion through differentially glycosylated EMMPRIN. J. Mol. Cell Biol. *7*, 143–153.

42. Janowska-Wieczorek, A., Marquez-Curtis, L.A., Wysoczynski, M., and Ratajczak, M.Z. (2006). Enhancing effect of platelet-derived microvesicles on the invasive potential of breast cancer cells. Transfusion *46*, 1199–1209.

43. Soares, K.C., Foley, K., Olino, K., Leubner, A., Mayo, S.C., Jain, A., Jaffee, E., Schulick, R.D., Yoshimura, K., Edil, B., and Zheng, L. (2014). A preclinical murine model of hepatic metastases. J. Vis. Exp. 51677.

44. Ponz-Sarvise, M., Tuveson, D.A., and Yu, K.H. (2015). Mouse models of pancreatic ductal adenocarcinoma. Hematol. Oncol. Clin. North Am. *29*, 609–617.

45. Hingorani, S.R., Wang, L., Multani, A.S., Combs, C., Deramaudt, T.B., Hruban, R.H., Rustgi, A.K., Chang, S., and Tuveson, D.A. (2005). Trp53R172H and KrasG12D cooperate to promote chromosomal instability and widely metastatic pancreatic ductal adenocarcinoma in mice. Cancer Cell *7*, 469–483.

46. Sadekar, S., and Ghandehari, H. (2012). Transepithelial transport and toxicity of PAMAM dendrimers: implications for oral drug delivery. Adv. Drug Deliv. Rev. *64*, 571–588.

47. Wang, J.G., Geddings, J.E., Aleman, M.M., Cardenas, J.C., Chantrathammachart, P., Williams, J.C., Kirchhofer, D., Bogdanov, V.Y., Bach, R.R., Rak, J., et al. (2012). Tumor-derived tissue factor activates coagulation and enhances thrombosis in a mouse xenograft model of human pancreatic cancer. Blood *119*, 5543–5552.

48. Yu, L.X., Yan, L., Yang, W., Wu, F.Q., Ling, Y., Chen, S.Z., Tang, L., Tan, Y.X., Cao, D., Wu, M.C., et al. (2014). Platelets promote tumour metastasis via interaction between TLR4 and tumour cell-released high-mobility group box1 protein. Nat. Commun. *5*, 5256.

49. Demers, M., and Wagner, D.D. (2014). NETosis: a new factor in tumor progression and cancer-associated thrombosis. Semin. Thromb. Hemost. *40*, 277–283.

50. Cedervall, J., Zhang, Y., and Olsson, A.-K. (2016). Tumor-induced NETosis as a risk factor for metastasis and organ failure. Cancer Res. *76*, 4311–4315.

51. Erpenbeck, L., and Schön, M.P. (2016). Neutrophil extracellular traps: protagonists of cancer progression? Oncogene *36*, 2483–2490.

52. Khorana, A.A., Mangu, P.B., Berlin, J., Engebretson, A., Hong, T.S., Maitra, A., Mohile, S.G., Mumber, M., Schulick, R., Shapiro, M., et al. (2016). Potentially curable pancreatic cancer: American Society of Clinical Oncology clinical practice guideline. J. Clin. Oncol. *34*, 2541–2556.

53. Sawabata, N., Okumura, M., Utsumi, T., Inoue, M., Shiono, H., Minami, M., Nishida, T., and Sawa, Y. (2007). Circulating tumor cells in peripheral blood caused by surgical manipulation of non-small-cell lung cancer: pilot study using an immunocytology method. Gen. Thorac. Cardiovasc. Surg. *55*, 189–192.

54. Jain, S., Pitoc, G.A., Holl, E.K., Zhang, Y., Borst, L., Leong, K.W., Lee, J., and Sullenger, B.A. (2012). Nucleic acid scavengers inhibit thrombosis without increasing bleeding. Proc. Natl. Acad. Sci. USA *109*, 12938–12943.

55. Stein, P.D., Beemath, A., Meyers, F.A., Skaf, E., Sanchez, J., and Olson, R.E. (2006). Incidence of venous thromboembolism in patients hospitalized with cancer. Am. J. Med. *119*, 60–68.

56. Zuckerman, J.E., and Davis, M.E. (2015). Clinical experiences with systemically administered siRNA-based therapeutics in cancer. Nat. Rev. Drug Discov. *14*, 843–856.

57. Holl, E.K., Shumansky, K.L., Pitoc, G., Ramsburg, E., and Sullenger, B.A. (2013). Nucleic acid scavenging polymers inhibit extracellular DNA-mediated innate immune activation without inhibiting anti-viral responses. PLoS One *8*, e69413.

58. Celiz, A.D., Smith, J.G.W., Patel, A.K., Hook, A.L., Rajamohan, D., George, V.T., Flatt, L., Patel, M.J., Epa, V.C., Singh, T., et al. (2015). Discovery of a novel polymer for human pluripotent stem cell expansion and multilineage differentiation. Adv. Mater. *27*, 4006–4012.

59. Celiz, A.D., Smith, J.G.W., Patel, A.K., Langer, R., Anderson, D.G., Barrett, D.A., Young, L.E., Davies, M.C., Denning, C., and Alexander, M.R. (2014). Chemically diverse polymer microarrays and high throughput surface characterisation: a method for discovery of materials for stem cell culture†Electronic supplementary information (ESI) available. See DOI: 10.1039/c4bm00054dClick here for additional data file. Biomater. Sci. *2*, 1604–1611.

60. Cheng, H., Kastrup, C.J., Ramanathan, R., Siegwart, D.J., Ma, M., Bogatyrev, S.R., Xu, Q., Whitehead, K.A., Langer, R., and Anderson, D.G. (2010). Nanoparticulate cellular patches for cell-mediated tumoritropic delivery. ACS Nano *4*, 625–631.

61. Papalezova, K.T., Tyler, D.S., Blazer, D.G., 3rd, Clary, B.M., Czito, B.G., Hurwitz, H.I., Uronis, H.E., Pappas, T.N., Willett, C.G., and White, R.R. (2012). Does preoperative therapy optimize outcomes in patients with resectable pancreatic cancer? J. Surg. Oncol. *106*, 111–118.

YMTHE, Volume *26*

Supplemental Information

Polymer-Mediated Inhibition of Pro-invasive Nucleic Acid DAMPs and Microvesicles Limits Pancreatic Cancer Metastasis

Ibtehaj Naqvi, Ruwan Gunaratne, Jessica E. McDade, Angelo Moreno, Rachel E. Rempel, Douglas C. Rouse, Silvia Gabriela Herrera, David S. Pisetsky, Jaewoo Lee, Rebekah R. White, and Bruce A. Sullenger

Supplementary Materials and Methods:

Patient Blood Collection

With approval from the Duke University Institutional Review Board, blood was collected from patients with pancreatic cancer after presentation with localized (early stage) or advanced disease and—in patients with early stage disease—at various time points in their treatment course, including before and after neoadjuvant (preoperative) chemoradiation therapy, intraoperatively during surgical resection, and one week postoperatively. Neoadjuvant chemoradiation therapy consisted of 45-50 Gy of external beam radiation therapy delivered over approximately 5 weeks with concurrent oral capecitabine as a radiation sensitizer [62]. Patients with advanced disease had undergone a variety of therapies including chemotherapy and/or radiation therapy. Blood was collected into BD SST Vacutainer tubes, and the sample was spun at 1500 rpm for 5 min. The supernatant was collected and aliquoted as patient sera for use.

Reagents

Generation 3.0 polyamidoamine dendrimer solution (PAMAM-G3) was purchased from Sigma Aldrich Cat. # 412422). The TLR agonists CpG ODN 2006, CpG ODN 1826, ODN 2088, Poly I:C, LPS, and R848 were purchased from Invivogen.

Human PC Cell Lines

Human BxPC3, Panc1, MiaPaCa2, and AsPc1 pancreatic cancer cell lines were purchased from ATCC. The following cell growth media were used for each cell line: BxPC3 and AsPC1 (RPMI 1640 plus 1% L-glutamine, 1% penicillin-streptomycin, 10% heat inactivated FBS), Panc1 (DMEM-high glucose plus 10% non-heat inactivated FBS), and MiaPaCa2

(DMEM-high glucose plus 10% non-heat inactivated FBS, 2.5% equine serum, 1% penicillin-streptomycin).

Generation of KPC4580P Murine PC Cell Line

The KPC4580P murine PC cell line- derived from the KPC genetic mouse model of pancreatic ductal adenocarcinoma (a gift of Jen Jen Yeh MD)- was generated in the following manner. In compliance with the University of North Carolina IACUC protocols, mice with Cre-inducible Kras and p53 mutations, Cre-inducible luciferase expression, and a pancreas specific Cre promoter were bred to obtain LSL-$Kras^{G12D/+}$; LSL-$Trp53^{R172H/+}$; $PDX1^{Cre/+}$; LSL-$ROSA26^{Luc/+}$ mice. This combination promotes the development of pancreatic ductal adenocarcinoma, as published before [46], with the addition of luciferase expression [63], which allows for easier follow up of the mutated cells. After PCR confirmation of the alleles, the mice were followed for disease progression and body condition. Tumor size was determined by either palpation or ultrasound. Once the tumor reached the maximum allowed size or the mouse had reached a humane endpoint, the mouse was euthanized and tumors were excised. Upon removal, part of the tumor was cut into approximately 3mm pieces and rinsed with PBS containing 5X penicillin/streptomycin (500 IU/mL and 500µg/mL). The tissue was then incubated for 1 hour in a 0.1 U/ml collagenase and 0.8 U/ml dispase solution. After incubation, dissociation media was removed, remaining tumor pieces were minced further and the tissue was resuspended in DMEM, 10% FBS and 1X penicillin/streptomycin and seeded onto tissue culture treated plates. The cells were incubated at 37˚C in a humidified chamber with 5% CO_2 and standard tissue culture protocols were used for their culture. Trypsin-EDTA was used for subculturing the cells. Cre-mediated recombination was confirmed by detection of the HINDIII restriction site in

the mutant Kras allele [64], and by detection of bioluminescence by the addition of D-luciferin to live cells. Cell growth media for the KPC4580P cell line consisted of DMEM-F12 media plus 10% non-heat inactivated FBS.

Quantification of Cell-Free DNA, Nucleosome, and HMGB1 Levels

Total DNA was isolated from sera using the DNA Blood Mini Kit (Qiagen) and quantified using the PicoGreen Staining Kit (Life Technologies). Nucleosome levels were quantified using the Cell Death ELISA Plus Kit (Roche). HMGB1 levels were quantified using an ELISA kit (Chondrex).

TLR Activation Assays

HEK-Blue TLR 4 and 9 reporter cell lines were purchased from Invivogen and activation in response to control agonists or human sera was determined according to the manufacturer's instructions. These cells stably co-express a TLR gene and an NFkB-inducible SEAP (secreted embryonic alkaline phosphatase) reporter gene that can be monitored using SEAP detection media. Briefly, these cells were plated in 96-well, clear-bottom, flat-bottom plates at a density of 100,000 cells per well with at least 5 wells per condition. The cells were then treated for 18-24 hours with either 1) media alone, 2) a control agonist for each given TLR (LPS [1 μg/mL] for TLR 4 and CpG ODN [5 μM] for TLR 9), 3) cancer patient sera [3.5 μL], 4) normal human sera [3.5 μL], 5) media alone + PAMAM-G3 [20 μg/mL], 6) control agonist + PAMAM-G3 [20 μg/mL], 7) cancer patient sera [3.5 μL] + PAMAM-G3 [20 μg/mL], or 8) normal patient sera [3.5 μL] + PAMAM-G3 in a final volume of 100 μL. After this incubation period, the cell supernatant was collected and mixed with Quantiblue (Invivogen) at a 60:40 vol:vol ratio and

incubated for 5 hours at 37C in a new 96 well plate, after which time absorbance at 650 nm was measured using a Spectramax i3 plate reader (Molecular Devices).

Microparticle and Exosome Isolation from Cultured PC cell lines and PC Patient Sera

KPC-4580P cells were cultured to confluence in T-175 flasks (Corning), at which time media was replaced with complete medium supplemented with exosome-depleted FBS instead of normal FBS. After 72 hours, the supernatant was collected and centrifuged at 4000g for 5 min to deplete cell debris. The residual supernatant was centrifuged at 20,000g for 20 min at 4C to pellet microparticles (MPs). The supernatant was removed and saved for exosome isolation. The MP pellet was washed with PBS (-/-) and re-centrifuged at 20,000g for 20 minutes at 4C. This supernatant was discarded and the final MP pellet was resuspended in 1mL of PBS, aliquoted and stored at -80 C. The supernatant from the initial MP spin was centrifuged at 100,000g for 2 hours at 4C to pellet exosomes. After discarding the supernatant, the exosome pellet was washed with PBS and this mixture was re-centrifuged at 100,000g for 2 hours at 4C. The supernatant was discarded and the exosome pellet was resuspended in 500 μL of PBS, aliquoted and stored at -80C. The protein concentration of the MPs and exosomes was quantified via Pierce BCA assay (Thermo-Fisher). To isolate MPs from human sera, sera was similarly centrifuged at 20,000 g for 20 minutes at 4C, supernatant was discarded, and resuspended in PBS.

Transwell-Matrigel Invasion Chamber Assays

Transwell-Matrigel invasion chambers were purchased from Corning and assays were performed according to the manufacturer's instructions. Briefly, the invasion chambers were first incubated with serum-free media in the top and bottom chambers at 37C for a minimum of 1.5

hours to allow the matrigel to solidify and the two chambers to equilibrate in preparation for the addition of PC cells and various agonists and/or inhibitors such as CpG ODN, PC cell line derived MPs and exosomes, PAMAM-G3, and ODN 2088. The human (BxPC3, MiaPaca2, PANC-1, AsPC-1) or mouse (KPC-4580P) PC cell lines were trypsinized, resuspended, and diluted in serum free media. After aspiration of media from both chambers, cells were plated in the top chamber at a density of 50,000 cells/well (500 μL final volume) in the presence of serum free media alone or various combinations of agonists and/or PAMAM-G3 [20 μg/mL] or ODN 2088 [100 μM]. Agonists tested included CpG ODN [5 μM], PC cell line derived MPs or exosomes (isolated as described above), PC patient sera or normal human sera (50 μL), or mouse sera (45 μL). 750 μL of complete media was added to the bottom chambers. All conditions were tested in duplicate. The plated invasion chambers were incubated at 37C for 24 hours, after which time media was aspirated from the top chambers. The top chambers were then removed and placed into a new 24-well plate preloaded with 1 mL of 10% formaldehyde per well to fix the invaded cells on the bottom surface of the chamber. After fixation for 10 minutes, the top chambers were then removed from the formaldehyde and placed into a new 24-well plate preloaded with 1 mL of PBS (-/-) per well for 1 minute for washing purposes. The top chambers were then placed onto absorbent pads and residual PBS was wiped from the inside of the top chambers using a cotton swab. 10 μL of crystal violet solution (5% w/v crystal violet, 25% v/v methanol) was added to the membranes and allowed to stain for 5 minutes. Crystal violet was from Sigma Aldrich. The chambers were then washed thoroughly in deionized water and residual crystal violet was wiped from the inside of the chambers using a cotton swab. The membranes were then imaged using an inverted light microscope (Olympus IX50) at 4X magnification. 10 random images of each membrane were taken using an eyepiece camera (Dino-Eye AM7023B).

The cells in the images were then counted using an ImageJ algorithm unique for each cell line (http://imagej.net/Particle_Analysis).

Analysis of Nuclear NFkB Translocation

KPC-4580P cells were plated at $2x10^6$ cells per plate in 35 mm plates overnight and BxPC3 cells were plated at $2x10^5$ cells per plate in 35 mm plates overnight. The cells were then treated with serum-free media alone, CpG ODN (1826 or 2006) [5 μM], or CpG [5 μM] and PAMAM-G3 [20 μg/mL] for 1 hour. Cell nuclei were then isolated using a nuclear isolation kit (Active Motif) using the manufacturer's guidelines. The protein content of each nuclear extract was quantified and standardized using a Protein Quantification Kit (Active Motif). The nuclear extract was then used to quantify nuclear translocation of NFkB via ELISA. For the murine nuclear extracts, nuclear translocation of p50 NFkB was quantified using the Pierce p50 Transcription Factor Assay Kit (Thermo Fisher) using the manufacturer's instructions. For the human nuclear extracts, nuclear translocation of p65 NFkB was quantified using the p65 TransAM ELISA (Active Motif).

Analysis of Cell Viability

In order to replicate conditions used for the invasion chamber assays, Panc1 or KPC4580P cells were seeded overnight in 96-well assay plates at a density of 50,000 cells/well. Panc1 cell were then treated with CpG ODN 2006 [5 μM], PAMAM-G3 [20 μg/mL], or media (4 wells per treatment group). After 24 hours, cell viability was measured according to the Cell Titer Glo Luminescent Cell Viability Assay (Promega), according to the manufacturer's instructions. KPC4580P cells were treated with CpG ODN 1826 [5 μM], KPC4580P-derived MPs (100

ng/μL), KPC4580P-derived exosomes (50 ng/μL), PAMAM-G3 [20 μg/mL], 1% Triton X-100, or media (12 wells per treatment group). After 24 hours, cell viability was measured according to the Cell Titer Glo Luminescent Cell Viability Assay (Promega), according to the manufacturer's instructions.

ELISA for Detection of PAMAM-G3 Binding to MPs

The binding of MPs and exosomes to PAMAM-G3 was quantified using a custom-designed ELISA assay. MPs and exosomes were isolated from KPC4580P PC cell cultures as described above. 96-well high binding, flat bottom plates (Corning) were coated overnight at 4C with PAMAM-G3 diluted into PBS (-/-) at varying concentrations (0, 0.2, 2, or 20 μg/mL) in duplicate rows (100 μL/well). The wells were washed 3 times with PBS and incubated for 2 hours at RT with blocking buffer (PBS plus 5% bovine serum albumin and 0.05% Tween-20). After washing 3 times with PBS, the wells were incubated with varying concentrations of MPs or exosomes for 2 hours at RT. After washing 3 times with PBS, the wells were then incubated with either the polyclonal goat IgG against murine tissue factor (AF3178, R&D Systems) for MP detection or the monoclonal mouse IgG antibody against phosphatidylserine (05-719, Millipore) for exosome detection. Both antibodies were used at a 1:1000 dilution in PBS plus 1% BSA and 0.05% Tween-20) and incubated for 1 hour at RT. After another 3 washes with PBS, the wells were incubated with the appropriate horseradish peroxidase-conjugated secondary antibody for 1 hour at RT. The wells were washed again 3 times with PBS. At this point TMB substrate (100 μL) was added to each well, and stop solution (100 μL) was added after 15 min. Absorbance at 450 nm was measured by a Spectramax i3 plate reader (Molecular Diagnostics). The binding of PC patient-derived MPs to PAMAM was quantified analogously. MPs were isolated from pooled

patient sera by centrifugation at 20,000g for 20 min at 4C, and the ELISA procedure was followed as described above using the anti-phosphatidylserine primary antibody for MP detection.

Syngeneic Murine Model of Pancreatic Cancer Metastasis

All animal experiments were performed in compliance with Duke IACUC protocols. Briefly, for metastasis studies, KPC4580P luciferase expressing, murine PC cells (described above) were surgically implanted into the spleens of 12 week old female C57BL6 mice. Starting on Day 2 after tumor cell implantation, mice were treated twice per week with either intraperitoneal PAMAM-G3 (20 mg/kg) or saline for 4 weeks or until humane endpoints were reached, at which time the mice were sacrificed. Liver and spleen were harvested from each mouse for assessment of gross organ weight and *ex vivo* quantification of bioluminescent intensity (IVIS Kinetic). Just prior to sacrifice, caudal vena cava blood was collected from each mouse for analysis of blood cell counts (Heska HemaTrue blood analyzer), plasma cfDNA (described above), nucleosome levels (described above), HMGB1 levels (described above), or chemistry (performed by Duke DLAR Veterinary Diagnostic Lab), or for serum invasion assays (described above). For PAMAM-G3 toxicity studies, 12 week old female C57BL6 mice were treated twice per week with either intraperitoneal PAMAM-G3 (20 mg/kg) or saline for 3 weeks, at which time the mice were sacrificed. Just prior to sacrifice, submandibular blood was collected from each mouse for blood cell count analysis or plasma chemistry analysis as described above.

A more detailed description of the above procedure for tumor cell implantation now follows. KPC4580P cells were cultured to confluence, trypsinized, washed three times with sterile PBS, and resuspended in 1:1 (vol/vol) media:matrigel for a total injection volume of 50

μL (100,000 cells/mouse) and kept on ice prior to surgery. Matrigel matrix (growth factor reduced, phenol red free) was purchased from Corning. Anesthesia was induced with 3 to 5% isoflurane inhaled in a sealed chamber 3-5 minutes or until effect. After induction, each mouse was moved to dedicated prep station and placed in dorsal recumbency on a heating pad, while maintaining anesthesia with 1-3% isoflurane delivered by a nose cone. Lubricant was applied to the eyes to prevent dessication. Hair was removed from the ventral abdomen by shaving. Buprenorphine (0.10 mg/kg) was administered subcutaneously for analgesia. The surgical site on the abdomen was prepped with a povidone/iodine skin scrub followed by an alcohol rinse with sterile gauze, a total of three times. At this time, the mouse was moved to a dedicated surgical station, with anesthesia maintained with 1-3% isoflurane delivered by a nose cone and body temperature maintained at approximately 37°C with a Physitemp TCAT-2DF. The mouse was then placed in right lateral recumbency. Using sterile microscissors, an approximately 1.5 cm longitudinal incision was made in the skin, 1-cm left, lateral of midline, slightly medial to the spleen. Next a 1.5-cm incision was made in the abdominal musculature, mirroring the overlying superficial incision. The spleen was located using forceps and gently removed from the abdominal cavity. The cell suspension was carefully injected into the spleen using a sterile 29G needle syringe. Once the cells were injected, the needle was kept in the spleen for 60 seconds so that the matrigel solidified, ensuring that the cells did not leak into the abdominal cavity. The needle was removed, and the spleen was gently internalized using blunt tipped forceps. The abdominal musculature was closed using a 6-0 absorbable suture with an interrupted stitch. Prior to skin closure, the mouse was dosed with 2 mg/kg bupivacaine via syringe between the abdominal and cutaneous layers to ensure proper analgesia. The overlying skin was closed using a skin staple. At this point the mouse was removed from the inhaled anesthetic. The mouse was

allowed to recover in its cage with free access to food and water. All mice received subcutaneous buprenorphine (0.1 mg/kg) 24 hours after surgery. Additionally, if any mice displayed signs of pain such as hunching, they were provided with subcutaneous buprenorphine every 12 hours as needed. In 7-10 days, once the surgical wound healed, the skin staples were removed.

Statistical Analysis

All data were plotted and analyzed using Graphpad Prism or JMP software. Data were all tested for normality prior to statistically analyses. If normally distributed, differences between groups were compared using a two-tailed student's t-test. If the data were not normally distributed, as in the case of the *in vivo* organ bioluminescence and gross weight data, statistical analysis between groups was performed using the Kruskal Wallis test.

Supplementary References

63. Safran, M, Kim, WY, Kung, AL, Horner, JW, DePinho, RA, and Kaelin, WG (2003). Mouse reporter strain for noninvasive bioluminescent imaging of cells that have undergone Cre-mediated recombination. *Molecular imaging* **2**: 297-302.
64. Aguirre, AJ, Bardeesy, N, Sinha, M, Lopez, L, Tuveson, DA, Horner, J*, et al.* (2003). Activated Kras and Ink4a/Arf deficiency cooperate to produce metastatic pancreatic ductal adenocarcinoma. *Genes & Development* **17**: 3112-3126.

Supplementary Figure 1

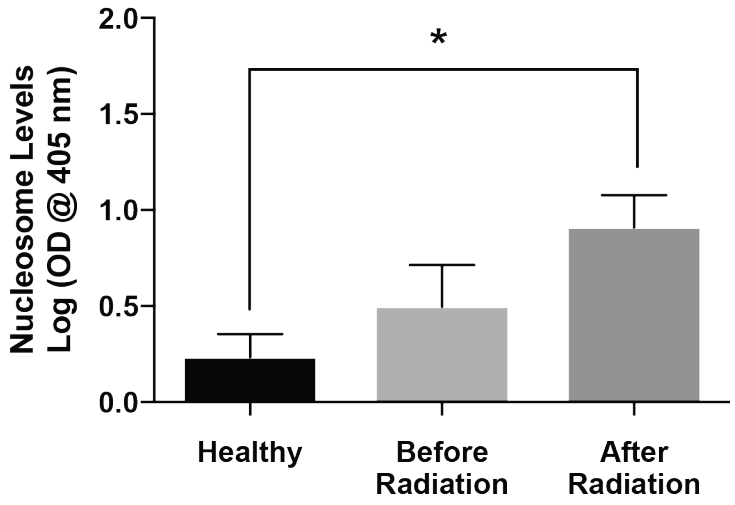

Figure S1. Circulating nucleosome levels are elevated in pancreatic cancer patients and further elevated after chemoradiation therapy (CRT). Serum nucleosome levels in healthy individuals and pancreatic cancer (PC) patients with localized, early stage disease before and after CRT (N = 8 for all groups), as measured by ELISA. * denotes $p < 0.05$ by two-tailed t-test. Raw data were log-transformed in order to satisfy normality requirement for parametric analysis by two-tailed t-test.

Supplementary Figure 2

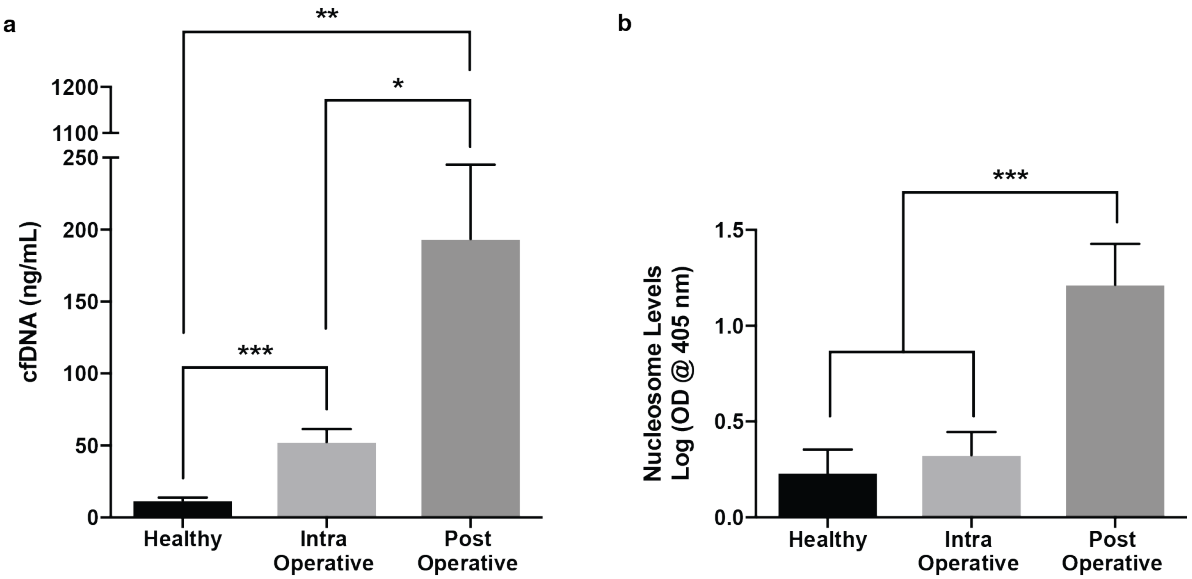

Figure S2. Elevation in serum cfDNA and nucleosome levels in pancreatic cancer patients during and after surgery. Serum cfDNA (a) and nucleosome (b) levels in healthy individuals and pancreatic cancer (PC) patients before and after surgical resection therapy, as measured by Picogreen staining and nucleosome ELISA respectively. N = 6 for all samples. ***, **, and * denote $p < 0.001$, $p < 0.01$, and $p < 0.05$ respectively by two-tailed t-test.

Supplementary Figure 3

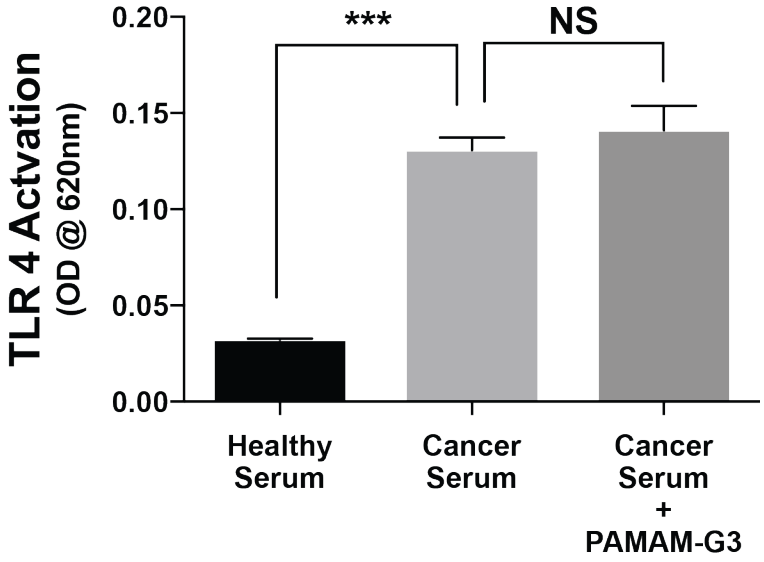

Figure S3. Pancreatic cancer patient serum activates TLR 4 but these effects are not inhibited by PAMAM-G3. TLR 4 activation by healthy human or pancreatic cancer (PC) patient sera in TLR 4 specific reporter cells, and effect with PAMAM-G3 (20 μg/mL) treatment. Individual experiments were performed with serum from two different PC patients and figure depicts a single representative experiment. *** and NS denote $p < 0.001$ and "not significant" respectively by two-tailed t-test.

Supplementary Figure 4

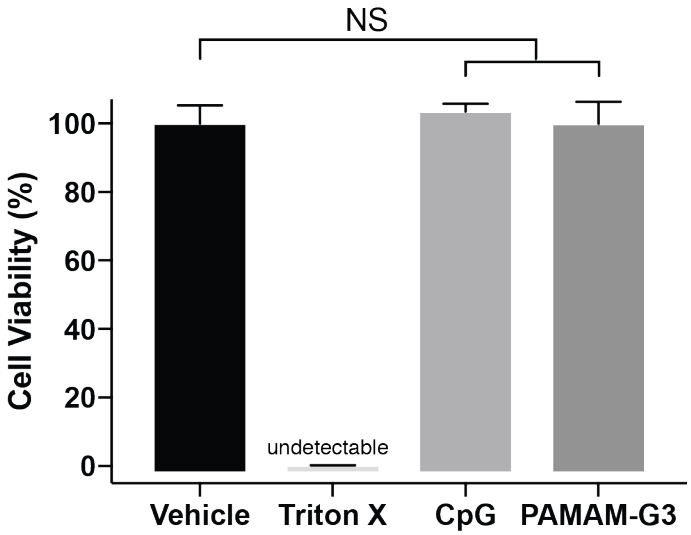

Figure S4. Treatment of pancreatic cancer (PC) cells with CpG ODN or PAMAM-G3 does not affect cell proliferation. Cell viability as measured by Cell-Titer Glow assay was determined after incubation of KPC4580P murine PC cells with media (vehicle), 1% Triton X-100, CpG ODN 1826 (5 μM), or PAMAM-G3 (20 μg/mL), for 24 hours. NS = not significant by two-tailed t-test.

Supplementary Figure 5

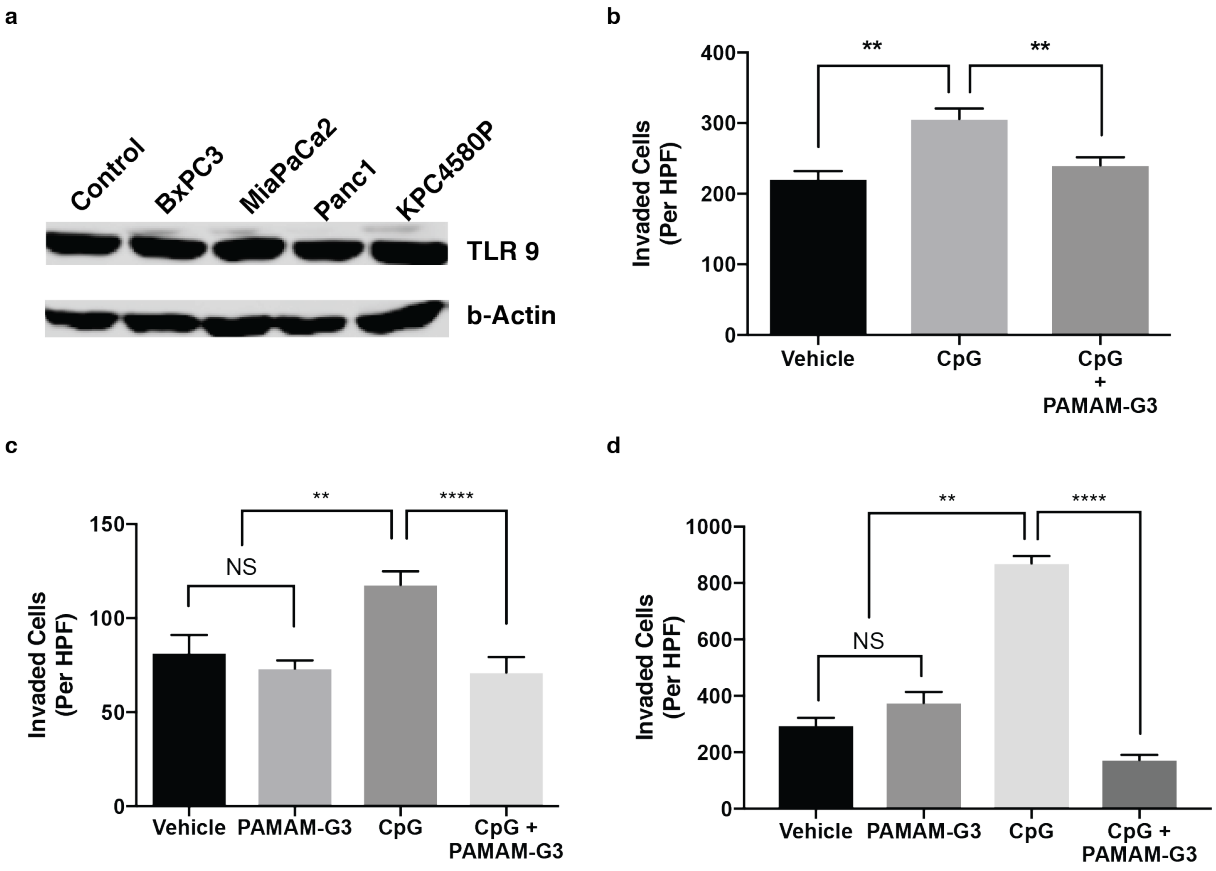

Figure S5. PAMAM-G3 inhibits CpG ODN induced invasion in human and murine pancreatic cancer cell lines. (a) Western blot expression of TLR 9 by a panel of human (BxPC3, MiaPaCa2) and murine (KPC4580P) pancreatic cancer cell lines. **(b-c)** Invasion of BxPC3 (b) and MiaPaCa2 (c) cell lines upon treatment with human TLR9 specific agonist CpG ODN 2006 (5 μM) in the absence or presence of PAMAM-G3 (20 μg/mL). **(d)** Invasion of KPC4580P cells upon treatment with the murine TLR9 specific agonist CpG ODN 1826 (5 μM) in the absence or presence of PAMAM-G3 (20 μg/mL). Effect of PAMAM-G3 (20 μg/mL) alone on cell invasion is also shown. ****, **, and NS denote $p < 0.0001$, $p < 0.01$, and "not significant" by two-tailed t-test. All invasion experiments were repeated at least three times and each bar graph depicts mean ± SEM of a single representative experiment.

Supplementary Figure 6

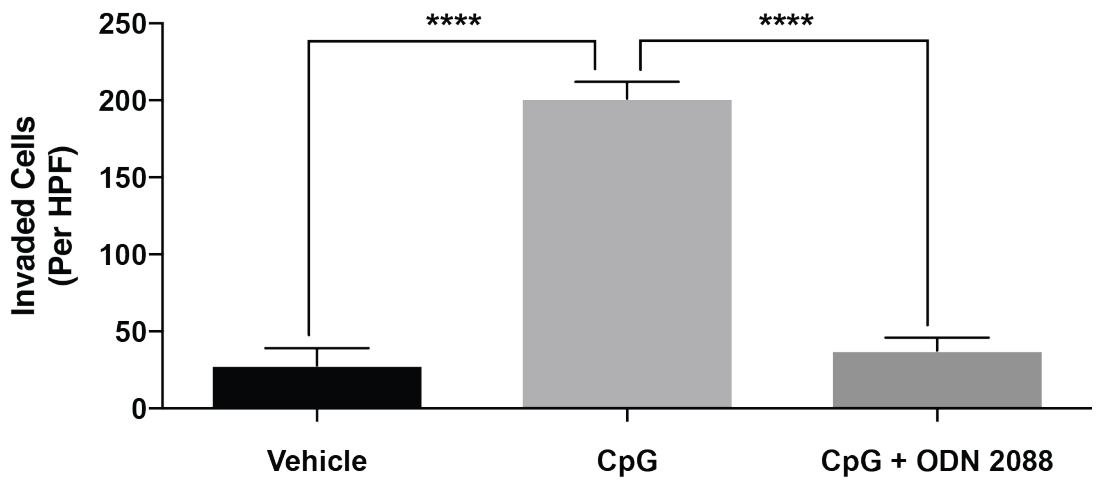

Figure S6. TLR 9 inhibitor, ODN 2088, inhibits CpG ODN induced invasion in pancreatic cancer cells. Invasion of KPC4580P cells upon treatment with human TLR 9 specific agonist CpG ODN 2006 (5 μM) in the absence or presence of the human TLR 9 specific oligonucleotide inhibitor ODN 2088 (100 μM). **** denotes $p < 0.0001$ by two-tailed t-test. Invasion experiment was repeated at least three times and each bar graph depicts mean ± SEM of a single representative experiment.

Supplementary Figure 7

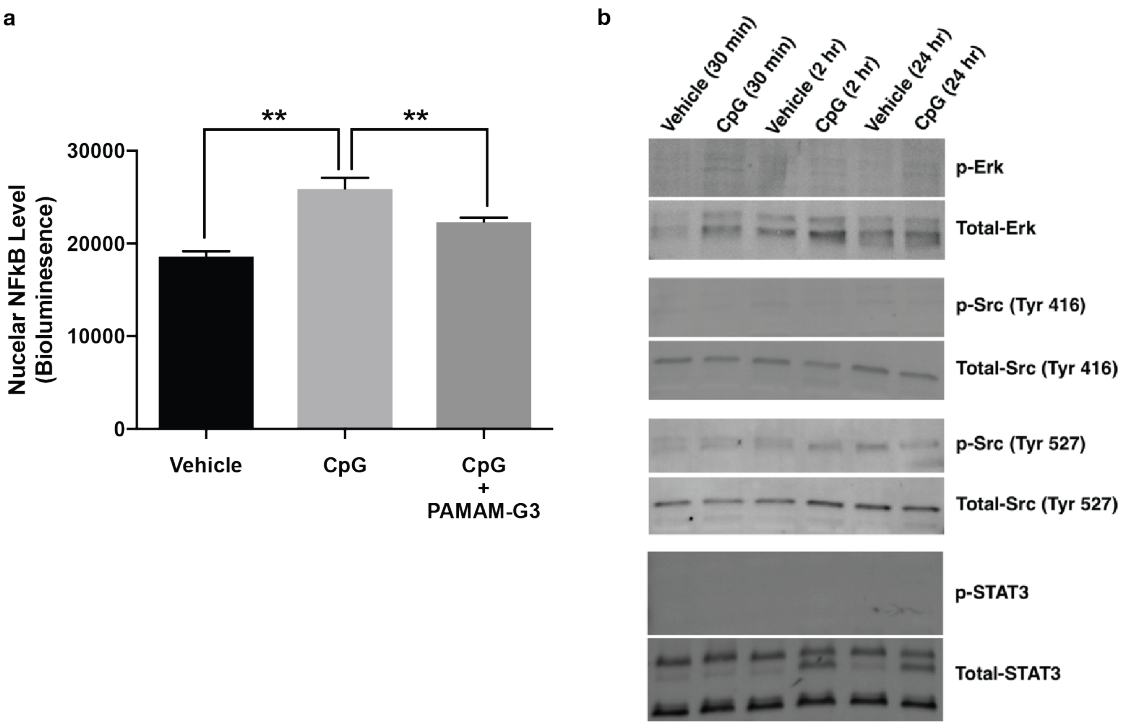

Figure S7. Addition of CpG ODN to PC cells increases nuclear translocation of p50 NFkB which is restored to baseline levels with PAMAM-G3 treatment, but does not activate the ERK, Src, and STAT3 signaling pathways. (a) Effect of CpG ODN 1826 (5 μM) treatment, alone or in combination with PAMAM-G3 (20 μg/mL), on nuclear translocation of NFkB in KPC4580P pancreatic cancer cells, as quantified by ELISA luminescent readout. Experiment was repeated three times and bar graph depicts mean ± SEM of a single representative experiment. ** denotes $p < 0.01$ by two-tailed t-test. (b) Effect of CpG ODN 1826 (5 μM) or vehicle (media) treatment on activation of the ERK, Src, and STAT3 signaling pathways as measured by phosphorylated ERK, Src (Tyr-416 or Tyr-527), and STAT3 detection by Western Blot in cell lysates collected at 30 min, 2 hr, or 24 hr post-treatment. Experiment was repeated three times and figure depicts a single representative experiment.

Supplementary Figure 8

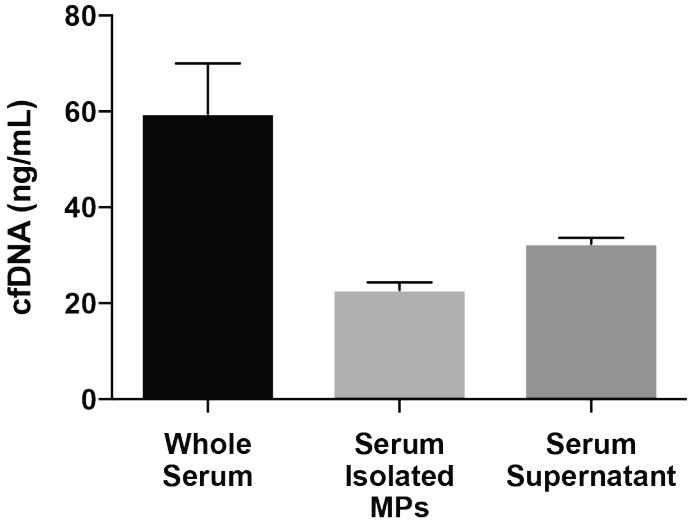

Figure S8. cfDNA in pancreatic cancer patient sera exists in both microvesicle bound and unbound forms. Pancreatic cancer patient serum was fractionated into microparticles and supernatant, and cell free DNA was quantified via PicoGreen staining after isolation with Qiagen's DNA Blood Mini Kit.

Supplementary Figure 9

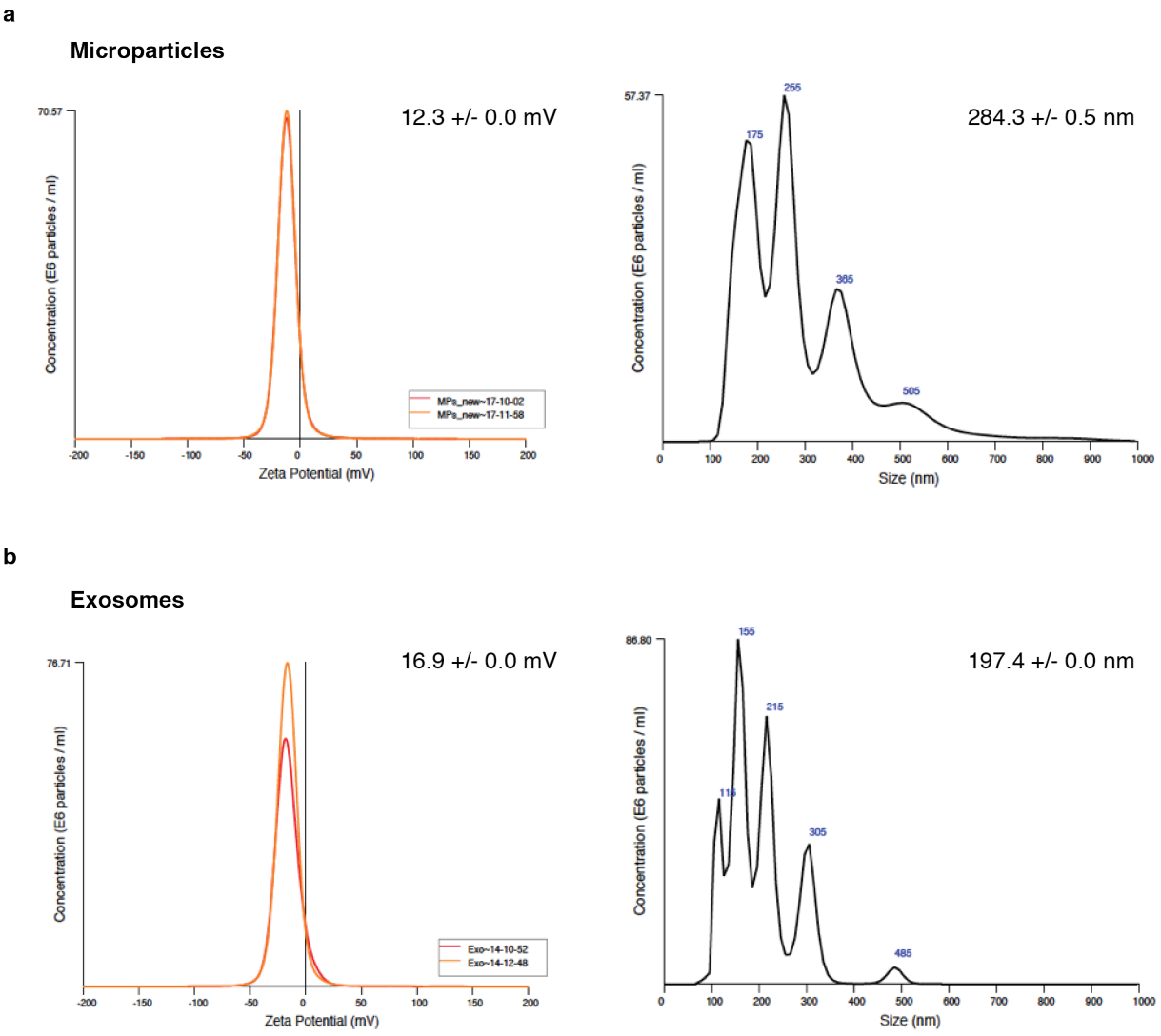

Figure S9. Pancreatic cancer derived microparticles and exosomes bear an electronegative surface charge. KPC4580P cell line derived microparticles (MPs) (a) and exosomes (b) were counted, sized, and analyzed for their surface charge using a Nanosight Zeta Potential Platform.

Supplementary Figure 10

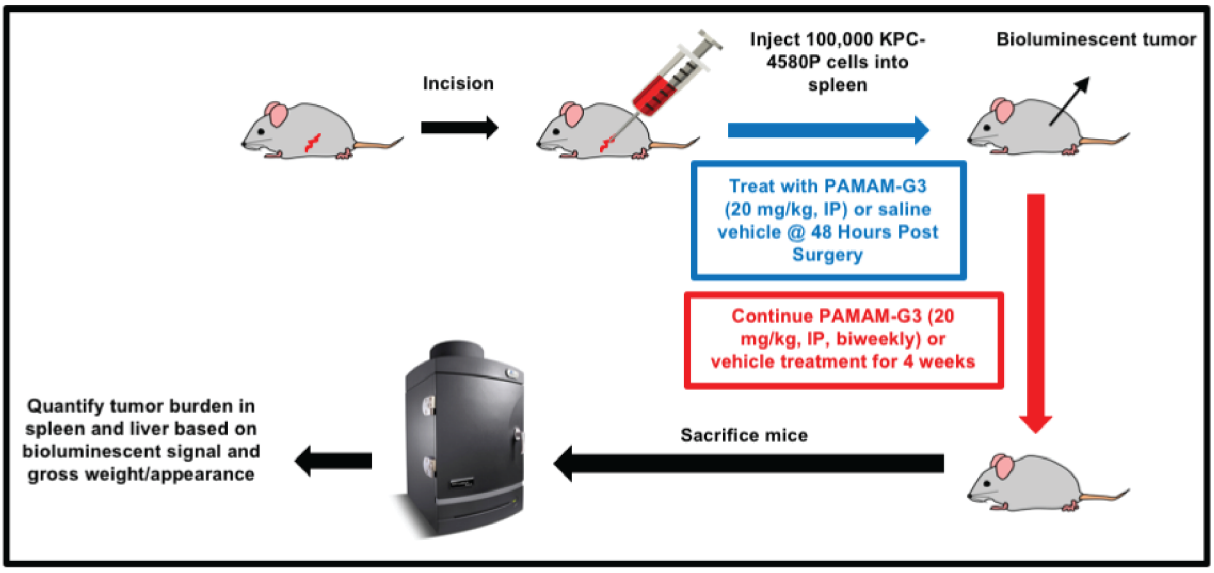

Figure S10. Experimental schematic of *in vivo* studies to evaluate the effect of PAMAM-G3 (G3) in a syngeneic murine model of pancreatic cancer metastasis. C57BL6 mice surgically implanted with 10^5 KPC4580P cells in their spleens reliably develop liver metastasis within 3-4 weeks. Groups of 25 mice were treated twice weekly with intraperitoneal injections of PAMAM-G3 (20 mg/kg) or saline vehicle starting 48 hours after tumor cell implantation. Primary (spleen) and metastatic (liver) tumor burden were quantified by measuring tumor specific *ex vivo* organ bioluminescence and weight after 4 weeks.

Supplementary Figure 11

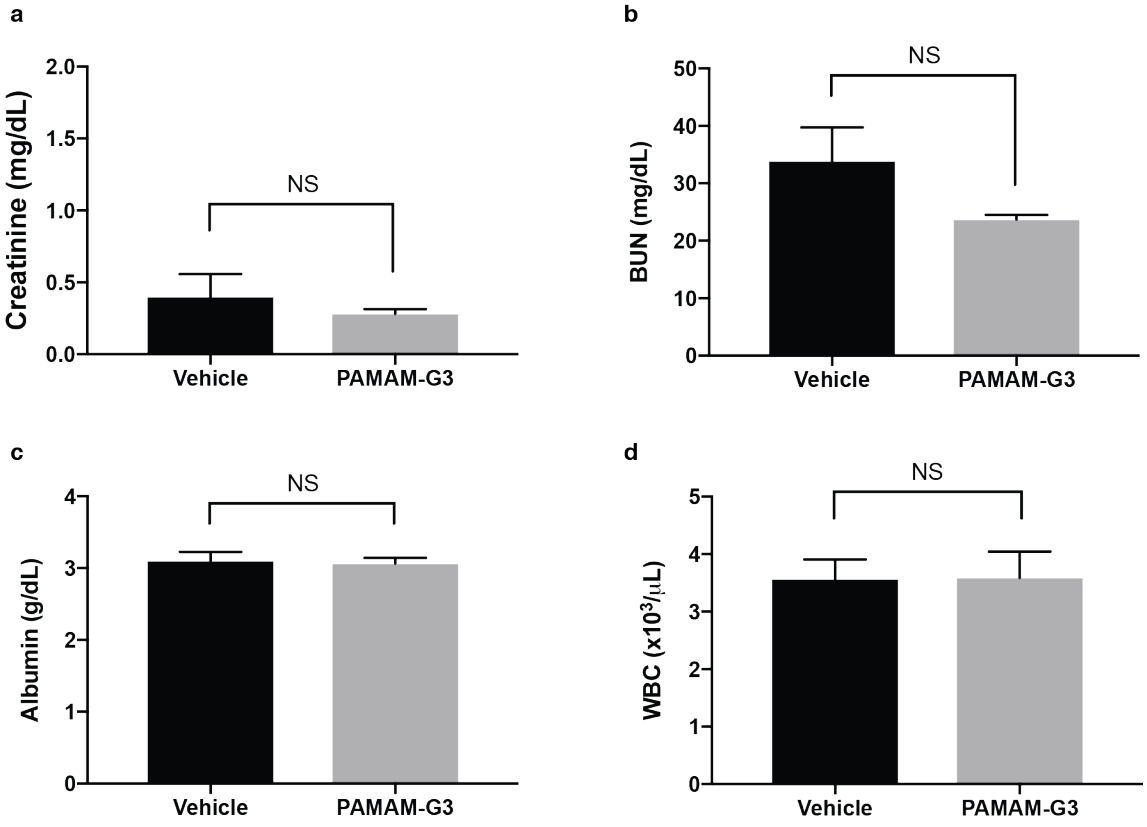

Figure S11. PAMAM-G3 administration in mice is not associated with changes in clinical chemistry values or blood cell counts that indicate systemic toxicity. Healthy, tumor-free C57BL6 mice were injected with PAMAM-G3 (20 mg/kg) (N = 9) or saline vehicle (N = 10) twice weekly for 3 weeks, after which time quantification of plasma creatinine (a), blood urea nitrogen (b), albumin (c), or white blood cell counts (d) was performed. Bar graphs depict mean ± SEM. NS denotes "not significant" by two-tailed t-test.